

EFFECTS OF CORROSION AND FATIGUE ON THE
LOAD-CARRYING CAPACITY OF STRUCTURAL
AND REINFORCING STEEL

Christopher Hahin, P.E. (Corrosion)
Engineer of Bridge Investigations
Illinois Department of Transportation
Springfield, Illinois 62704

1. Report No. FHWA/IL/PR- 108	2. Government Accession No.	3. Recipient's Catalog No.	
4. Title and Subtitle Effects of Corrosion and Fatigue on the Load Carrying Capacity of Structural and Reinforcing Steel		5. Report Date March, 1994	
7. Author(s) Christopher Hahin		6. Performing Organization Code	
9. Performing Organization Name and Address Illinois Department of Transportation Bureau of Materials and Physical Research 126 East Ash Street Springfield, Illinois 62704		8. Performing Organization Report No.	
12. Sponsoring Agency Name and Address* Illinois Department of Transportation Bureau of Materials and Physical Research, in cooperation with the U. S. Department of Transportation, Federal Highway Administration		10. Work Unit No. HR-25-317-94-1	
15. Supplementary Notes		11. Contract or Grant No.	
16. Abstract <p>Pitting and crevice corrosion have profound effects on the fatigue life of structural and reinforcing steels used in bridge construction. Stress concentration factors were measured on actual corroded plates with strain gage instrumentation. Using corrosion rates and pitting ratios for immersion, intermittent immersion and various atmospheric environments from the corrosion literature, a unified equation for corrosion fatigue of structural steels, $N = C/k_f[S_{corr}]^m$ is proposed to determine the number of stress cycles to significant crack formation. The coefficients C, k_f and m were determined in this investigation. Collected strain data is used to construct a stress-frequency histogram for a bridge, which establishes an accurate and rapid assessment of traffic damage. The linear damage rule is then used to integrate the simultaneous action of both mechanical fatigue and gradual surface degradation, and is combined with sectional loss from corrosion. The predictive equations developed in this report are very useful in the determination of load-carrying capacity and fatigue damage of bridges. These factors are integral to the planning of improvements and maintenance, the granting of overload permits, and for maximum load rating of bridges.</p>		13. Type of Report and Period Covered Final Report; July 1991 - February 1994	
17. Key Words Pitting; corrosion, corrosion fatigue; structural steel; reinforcing steel; load-carrying capacity, moment of inertia; load histogram.		14. Sponsoring Agency Code	
19. Security Classif. (of this report) Not classified		20. Security Classif. (of this page) Not classified	
		21. No. of Pages	22. Price

FOREWORD

This report should be of interest to engineers involved in bridge design, planning, maintenance and inspection; consultants, and other technical personnel concerned with the life cycles of bridges.

NOTICE

The contents of this report reflect the views of the authors who are responsible for the facts and the accuracy of the data presented herein. The contents do not necessarily reflect the official views or policy of the Federal Highway Administration or the Illinois Department of Transportation. This report does not constitute a standard, specification, or regulation.

Neither the United States Government nor the State of Illinois endorses products or manufacturers. Trade or manufacturer's names appear herein solely because they are considered essential to the object of this report.

ACKNOWLEDGEMENTS

The author wishes to express his appreciation to the following individuals of the Illinois Department of Transportation who assisted in the completion of this research project: Messrs. Jeff South, George Maier, Perry Walter, Paul Jenkins, Harry Smith, Russ Gotschall, Ken Wyatt, Tom Courtney, and Eric Harm, and Ms. Beverly Buhrmester, all of the Central Bureau of Materials and Physical Research; also Messrs. James Threadgill of District 3 Construction; Forrest Greenawalt and Karl Keeney of District 1 Construction. Mr. Roger Dalton is Chief Engineer of District 3 and Mr. Duane Carlson is Chief Engineer of District 1 Construction. Mr. James G. Gehler is Chief Engineer of the Bureau of Materials and Physical Research. The author also acknowledges the useful and productive discussions with Professor Pedro Albrecht of the University of Maryland and Professor Stan Rolfe of the University of Kansas regarding their relevant prior contributions to the corrosion fatigue literature.

This report represents the complete record of the experimental and theoretical studies performed by the author and those who assisted him, which are summarized in the conference paper of the same title published at the Structural Materials Technology Conference, Atlantic City, New Jersey, February 1994.

TABLE OF CONTENTS

INTRODUCTION.....	1
FATIGUE IN BRIDGES.....	4
Stress Ranges in Illinois Bridges.....	5
Determination of Fatigue Damage.....	12
Effects of Corrosion on Fatigue of Steel.....	17
Corrosion of Structural Steel.....	27
Effects of Corrosion on the Fatigue Failure Equation.....	30
STRESS CONCENTRATION AND FATIGUE STRENGTH.....	34
EFFECTS OF CORROSION ON THE MOMENT OF INERTIA.....	53
Moment of Inertia by Deflection.....	53
Moment of Inertia by Geometric Measurement.....	59
Effects of Atmospheric Corrosion and Deicers on Moment of Inertia.....	67
Effects of Pitting on the Fatigue of Structural Shapes.....	74
EFFECTS OF CORROSION ON THE LOAD-CARRYING CAPACITY OF REINFORCING BARS.....	75
Depth of Pitting and Weight Loss.....	76
Mechanical Properties Predicted by Composition.....	78
Weight Losses and Mechanical Property Losses.....	83
COMBINED EFFECTS OF CORROSION AND FATIGUE.....	90
Definition of S_{corr}	90
Structural Shapes in Bending.....	91
Plates or Shapes in Tension.....	92
Reinforcing Bars.....	93
Cumulative Fatigue Damage.....	94
Determination of Fatigue Damage of Corroded Members.....	95
SUMMARY AND CONCLUSIONS.....	101
REFERENCES.....	104

LIST OF FIGURES AND TABLES

- Figure 1. Stress-frequency histogram for US 12 & 45, Mannheim Road near Chicago O'Hare Airport (legal loads only).
- Figure 2. Composite histogram for the State of Illinois, based on 15 representative bridges.
- Figure 3. Stress-frequency histogram for US 12 & 45 showing legal loads and permit loads over 80,000 lbs. for a one month period.
- Figure 4. Fatigue data for carbon steel beams exposed to Maryland weather for 25 years.
- Figure 5. Fatigue data for weathering steel exposed to air and moist environments for 5.7 years in Maryland.
- Figure 6a/b. Pitting factor for carbon and weathering steel beams.
- Figure 7. Plots of corrosion fatigue data of many investigators.
- Figure 8. Dimensions and pitting in specimen A.
- Figure 9. Dimensions and pitting in specimen C1.
- Figure 10. Dimensions and pitting in specimen C2.
- Figure 11. Dimensions and pitting in specimen D2.
- Figure 12. Dimensions and pitting in specimen E1.
- Figure 13. Dimensions and pitting in specimen F1.
- Figure 14. Dimensions and pitting in specimen F2.
- Figure 15. Dimensions and pitting in specimen F3.
- Figure 16. Dimensions and pitting in specimen G1.
- Figure 17. Dimensions and pitting in specimen G2.
- Figure 18. Dimensions and pitting in specimen G3.
- Figure 19. Typical strain gage mountings on corroded plates.
- Figure 20. Stress concentrations in pitted plates as a function of pit depth.
- Figure 21. Stress concentrations in corroded plates as a function of plate thickness and pit radius.

LIST OF FIGURES AND TABLES (CONT'D.)

- Figure 22. Overall view of test frame.
- Figure 23. Strain gage readout of stresses to correlate with deflection measured by dial indicator.
- Figure 24. Frame restraint to prevent block toppling.
- Figure 25. Simplified geometric method of determining moment of inertia.
- Figure 26. Effects of corrosion on an I-beam not painted for 25 years.
- Figure 27. Exfoliated rivet exposed to corrosion on bridge pier for 75 years.
- Figure 28. Effect of carbon content on the properties of hot worked plain carbon steels.
- Figure 29. Loss in yield strength in a reinforcing bar as a function of percent weight loss.
- Figure 30. Loss in ductility in a reinforcing bar as a function of percent weight loss.
- Figure 31. Maximum pit depth in reinforcing bars as a function of % weight loss.
- Figure 32. Stress concentrations in reinforcing bars as a function of yield strength and weight loss.
- Figure 33. Stress concentrations in a reinforcing bar as a function of tensile strength and weight loss.

LIST OF FIGURE AND TABLES (CONT'D.)

Table 1	Types of bridges and typical corrosion-prone areas.
Table 2	Characteristics of Illinois bridges studied.
Table 3	Fatigue strength coefficients and exponents for typical AWS fatigue stress categories.
Table 4	Calculations of cumulative damage by histogram-linear damage method.
Table 5	Fatigue strength of common structural steels in rotating bending.
Table 6	Atmospheric corrosion rates for various structural steels.
Table 7	Pit depths, radii, thickness and stress concentration for corroded plates.
Table 8	Summary of deflection data.
Table 9	Dimensions of corroded beams.
Table 10	Moment of inertia obtained by deflection under uniform load vs. mean geometric measurements.
Table 11	Corrosion and pitting rates of bridge steels in various locations.
Table 12	Pit depths vs. weight losses for #4 reinforcing bars.
Table 13	Predicted mechanical properties of reinforcing bars from composition.
Table 14	Effects of weight loss on mechanical properties of reinforcing bars.
Table 15	Effects on environment on fatigue coefficients for unpainted ASTM A588 girders.
Table 16	Damage comparison of whether unpainted weathering steel should be painted.

INTRODUCTION

Steel and reinforced concrete bridges are subject to various forms of deterioration by the simultaneous action of corrosion because of their location and environment, and by fatigue because of the moving loads they must carry. Bridges in Illinois may be located near or over large fresh water lakes or major rivers, or be in close proximity to industrial pollution or even dust-laden atmospheres. Bridges are subject to various forms of corrosion, including general corrosion, crevice and pitting corrosion, corrosion fatigue, and fretting corrosion. Sometimes stress corrosion cracking is occasionally encountered. If bridges are located in areas subject to freeze-thaw conditions, de-icing salts are often applied to their approaches or decking for skid protection of vehicles using the bridge. Loads on bridges vary from light passenger cars weighing only 2,000 lbs (8.9 kN) to heavy trucks up to 80,000 lbs (355.8 kN). Permit loads over and above 80,000 lbs on major truck routes are not unusual events for many bridges.

Depending on its location, a bridge may or may not be simultaneously sustaining both corrosion and cyclic fatigue on a continuous basis. The number of wet-dry cycles sustained by the bridge is a function of the climate of the location, and whether load-carrying members of the bridge are being subjected to moisture or saline media, and how rapidly they dry determines how much corrosion fatigue they sustain. Some members are continually or alternately immersed, such as steel pilings. The various types of bridges and their details that are typically

vulnerable to corrosion are summarized in Table 1. Many bridges in congested locations, however, do sustain mechanical fatigue on a continuous basis. Several bridge members may have formed cracks because of fatigue, whereas many others are sustaining cumulative fatigue damage without the appearance of an overt crack.

TABLE 1

Types of Bridges and Typical Corrosion-Prone Areas

<u>Type of Bridge</u>	<u>Structural Areas Subject to Corrosion</u>
1. Multi-girder, with welded plates & stiffeners (non-composite deck)	General attack; pitting & crevice corrosion at diaphragms, wide flange webs, upper & lower flanges; expansion joint leakage onto pier caps & rockers or bearings; corrosion of rebars & cracking of concrete.
2. Deck-multigirder composite	Deck cracking & rebar corrosion; pitting & section loss of girder webs & lower flanges; expansion joint leakage onto pier caps & bearings.
3. Girder-floor beam system	Crevice & pitting of floor beams & connections, stringers, & lateral bracing gussets, deck cracking; rebar corrosion; pier cap degradation.
4. Deck & truss	Floor beam degradation by pitting, section loss; deck cracking; section loss, pitting & general crevice corrosion of truss lower chords.
5. Tied arch	Crevice corrosion of cables & moorings & anchors; corrosion & fatigue of arch tie girders or box beams; deck cracking.
6. Trapezoidal or box girder	Internal drainage problems; leakage at expansion joints or cracked decks; corrosion fatigue of cracked stiffeners.
7. Bascule & vertical lift movable bridges	Corrosion of floor beams, structural members in counterweight or counterweight pit; pitting corrosion of exposed machinery; crevice corrosion in open grid decks.
8. Reinforced concrete	Deck cracking; spalling of concrete on piers and where reinforcement has minimal cover; pitting of rebar; loss of rebar development.

Bridge designs moved away from the older heavy riveting and bolting methods in the late 1950s toward the use of welded construction because of its simplicity, ease of assembly, and lower labor intensity. However, many welded structures have sustained cracking largely as a function of (1) poor design selection of weld detail or improper electrodes, (2) residual stresses derived from either insufficient preheat, poor fit-up and tolerances, or (3) construction practices which contribute to premature cracking. These weld failures are not typically corrosion-related, but are fatigue cracks that are largely mechanical in nature. This study was confined to the effects of fatigue damage to uncracked members that are slowly losing their structural properties by sustaining section loss by general corrosion and fatigue crack initiation life, which constitutes the vast majority of a bridge's fatigue life.

FATIGUE IN BRIDGES

Bridges sustain fatigue by the mechanical loadings of thousands of moving trucks and full size passenger cars passing over each year. Many compact and intermediate-sized passenger cars register stress ranges so insignificant that they often cannot be detected by strain gages because their signal amplitudes are roughly equal to or less than the electronic noise output of the circuitry of the measurement device. When a truck traverses a bridge, the main load-carrying members deflect

downward upon impact and reverse such deflection after passage of a truck over a pier if the bridge members are continuous. Typically, these registrable stress ranges are from 0.5 to 5.5 ksi (3.4–37.9 MPa). Although these stress ranges can be determined by analytical theory, such calculations are only indicative because they do not take unintended load sharing and fixities of connections into account. In addition, the mechanical properties of materials used in the construction may significantly exceed their minimum specified properties. If bridges are instrumented with foil strain gages, linear voltage differential transformers (LVDTs) or dial indicators or other means of determining strain, the actual stress ranges encountered at strategic locations on the bridge can be accurately measured and then compared with analytical calculations.

Stress Ranges in Illinois Bridges

Between July 1990 and July 1991, a total of 15 bridges representing various locations, different traffic densities, and other characteristics, were monitored throughout the State of Illinois.¹ The characteristics of those bridges are summarized in Table 2.

The bridges were instrumented with an array of foil strain gages at various locations, and data was acquired as a function of time. A variety of data acquisition systems are commercially available which gather and process the strain readings; in this study the DataMyte System of Minnetonka, MN was used.

The strain gage data was then sorted by a data processor into various stress ranges, forming a cumulative stress range-frequency histogram for that particular bridge. A histogram for the Mannheim Road bridge near O'Hare Airport in Franklin Park, Illinois is shown in Figure 1. A composite histogram based on the mean of each stress range for the 15 bridges is shown in Figure 2. This composite histogram provides a typical profile of stresses induced by traffic loading on bridges throughout the state and is useful for planning and taxation studies.

These histograms are based on stresses induced by so-called legal loads (trucks weighing 80,000 lbs [355.8 kN] or less). Trucks above the legal limit of 80,000 lbs are required to file a permit for passage over the bridge to ensure that permissible stresses are not exceeded. Figure 3 is stress frequency histogram for US 12 and 45 (Mannheim Road near O'Hare Airport) that shows legal loads plus all permit loads issued for the month of August, 1992. This histogram was constructed by assuming linear proportionality of the stresses induced by loads over and above 80,000 lbs. Preliminary investigations¹ indicate that both the upper and lower bounds of this linear extrapolation are within $\pm 10\%$.

TABLE 2

Characteristics of Illinois Bridges Studied

<u>Bridge No.</u>	<u>Type of Span</u>	<u>Bridge Location</u>	<u>ADT*</u>	<u>ADTT**</u>	<u>Location of Gages on Bridges</u>
0160158	Truss with simply supported approach spans	Calumet Expressway, Chicago	51,800	15,800	Main vertical trusses
0160335	Continuous span	US 12 & 45, Mannheim Road, near O'Hare	47,000	4,350	Ends of welded coverplates
016022	Overhead truss span with simply supported approaches	IL Route 83 over Cal-Sag Channel, metro Chicago	28,000	2,000	Midspan of rolled section main girder
0990055	Simply supported span	I-80 east-bound Joliet	21,000	8,550	Flange transition welds
1010019	3 span, continuous	US 20 over Grove Creek, near Rockford	4,150	900	Ends of welded coverplates
1010055/ 1010056	Continuous with cantilevered side spans	East & west-bound US 20 over IL 2, Rockford	6,400	900	Tensioned large hole in a pin plate
0570050	3 span, 2-girder span with floorbeams	US 51 over Mackinaw river, Bloomington	8,009	1,700	Ends of welded coverplate
0570067/ 0570068	Simply supported single spans	I-55 over Sugar Creek, Bloomington	13,400	850	Midspan of rolled section main girder
0720014	3 span continuous	IL 29 over Senechwine Creek, Chillicothe	6,400	500	Ends of welded coverplates
0540031	Continuous steel girders	IL 54 over Lake Fork Creek, near Springfield	1,150	125	Ends of welded coverplates

TABLE 2 (CONTINUED)

Characteristics of Illinois Bridges Studied

<u>Bridge No.</u>	<u>Type of Span</u>	<u>Bridge Location</u>	<u>ADT*</u>	<u>ADTT**</u>	<u>Location of Gages on Bridges</u>
0650005	Continuous steel girders	IL 97 over C&IM RR near Petersburg	2,900	200	Ends of welded coverplates
0420017	Continuous steel girders	US 67 over Macoupin Creek near Rockbridge	1,750	375	Ends of welded coverplates
0600126	Riveted continuous girders	IL 111 over Cahokia Canal near Fairmont City	3,400	850	Ends of riveted coverplates

*ADT = Average Daily Traffic

**ADTT = Average Daily Commercial Truck Traffic

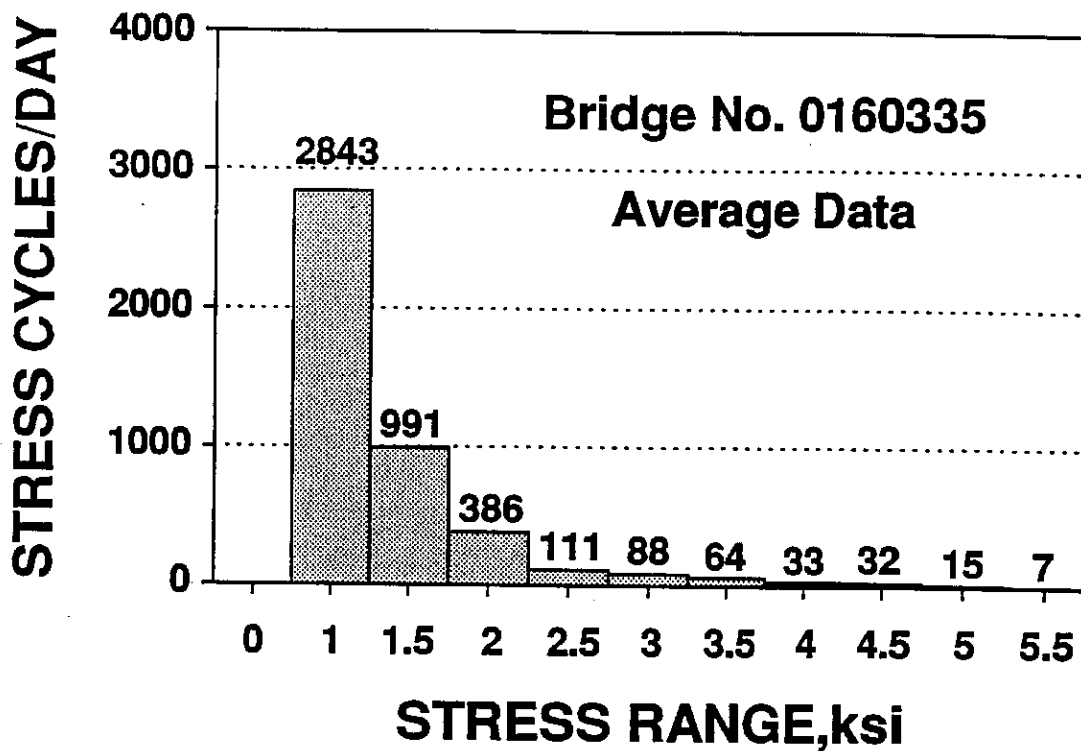


Figure 1. Stress range-frequency histogram for a major metropolitan feeder route, US 12 & 45 (Mannheim Road near O'Hare Airport), carrying a large traffic volume, and a full spectrum of light-to-heavy commercial vehicles. Data of Hahin and South¹.

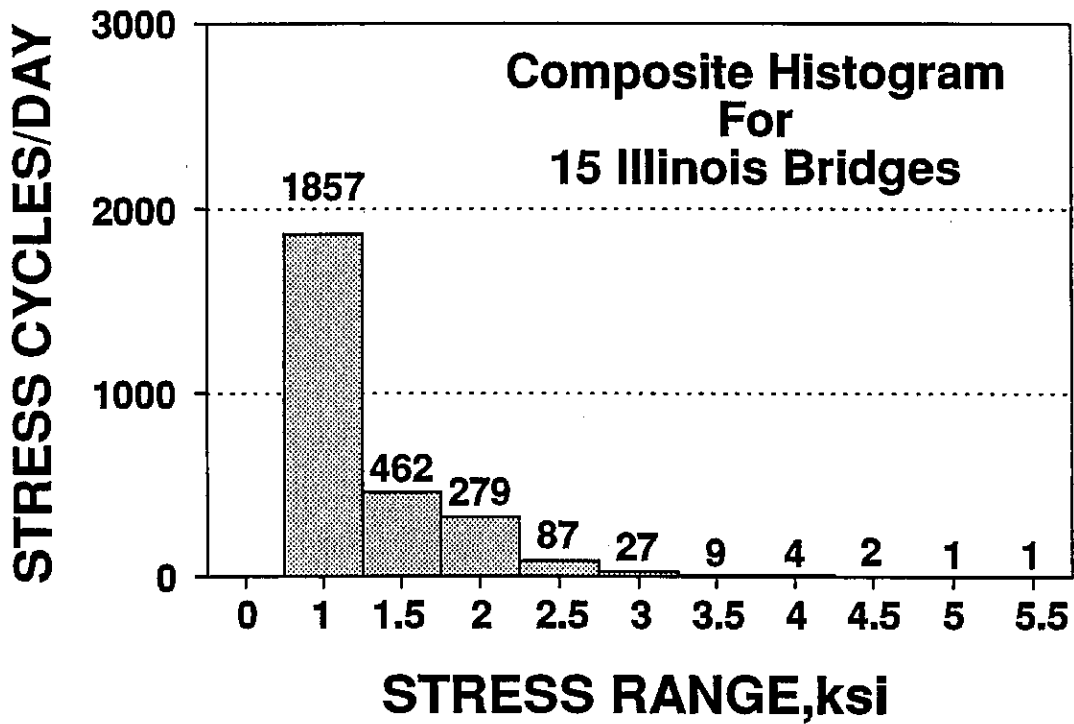


Figure 2. Composite stress range vs. frequency histogram for the State of Illinois, based on a mean of each stress range and frequency for 15 representative bridges. Data of Hahin and South¹.

Bridge No. 0160335 Average Data

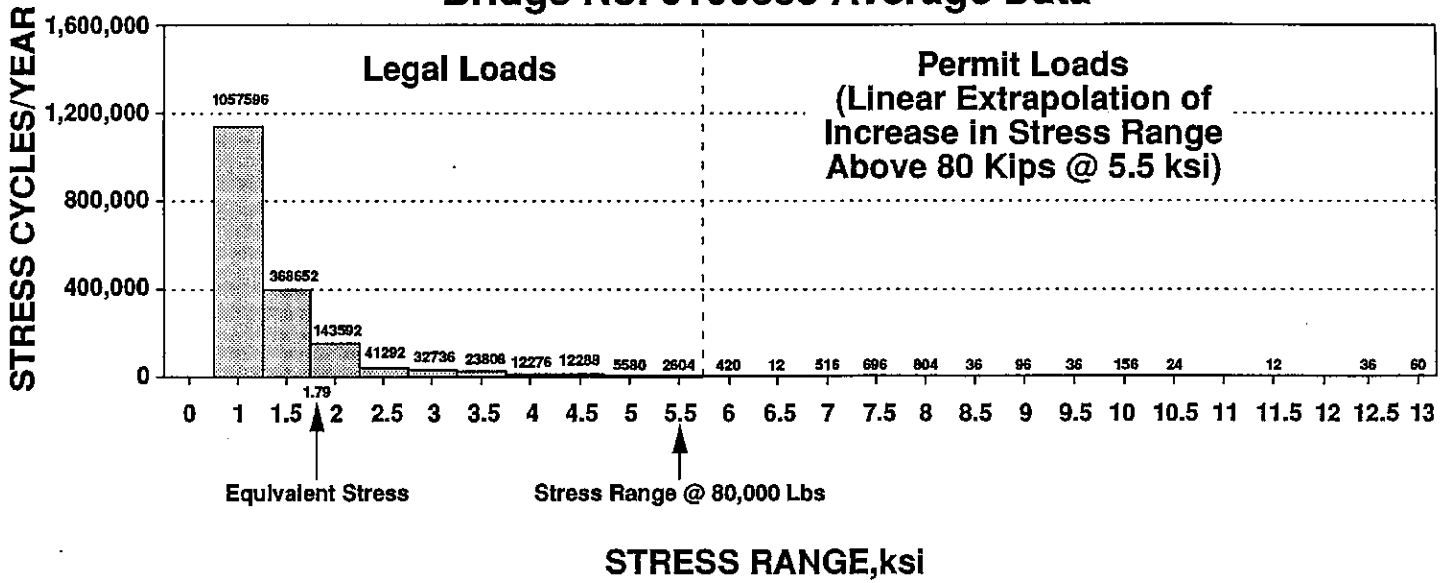


Figure 3. The number of stress cycles at 0.5 ksi (3.4 MPa) increments for legal loads to 5.5 ksi (37.9 MPa) and permit loads above 80,000 lbs (355.8 kN) for Mannheim Road Bridge (US 45) near Franklin Park, Il., south of O'Hare Airport. Data of Hahin and South¹.

Determination of Fatigue Damage

Using the stress range-frequency histogram obtained from a bridge in question, the amount of fatigue damage that the bridge will sustain in one year is calculated. When collecting stress range data on a bridge, it is best to monitor traffic for an entire 7-day week. If the truck traffic changes on a seasonal basis, which is typically the case for certain rural roads, stress range data should be sampled for several weeks that are scattered throughout the entire year. The number of cycles sustained by a particular critical or main load-carrying detail for each stress range is totaled for one week of exposure to traffic and multiplied by 52, the number of weeks in a year.

The stress range frequency histogram now represents the cumulative damage sustained by that particular bridge detail in one year. Depending on the member or the weld detail in question, the cumulative damage is then compared with AWS/AASHTO stress vs. number of cycles charts using the linear damage rule:

$$\sum \frac{n_{sri}}{N_{sri}} = \frac{n_{sr1}}{N_{sr1}} + \frac{n_{sr2}}{N_{sr2}} + \frac{n_{sr3}}{N_{sr3}} + \dots = 1 \quad \text{[Equation 1]}$$

where: n_{sri} = number of stress cycles per year at a specific stress interval (0.5 ksi [3.4 MPa] in this study)

N_{sri} = number of stress cycles sustainable at this stress range per AWS/AASHTO fatigue category to cause cracking

The linear damage rule has been widely used in fatigue studies because of its accuracy and simplicity in handling the statistical nature of fatigue.

The AWS/AASHTO fatigue categories in S-N form (stress vs. number of cycles) can be rearranged into a more convenient $N = f(S)$ form:

$$N_{sr} = C[S]^m \quad \text{[Equation 2]}$$

where: S = stress range, ksi
 C = fatigue strength coefficient
 m = fatigue strength exponent
 N_{sr} = number of cycles to major crack formation at
a particular stress range

The fatigue strength coefficients and exponents for AWS/AASHTO fatigue categories A through E for redundant and non-redundant structures are summarized in Table 3. In general, the fatigue exponent m varies between 2.9 and 3.8 with few exceptions. Most of the fatigue category lines are largely parallel, with the mean slope for redundant and non-redundant classifications both combined is $m = -3.26$.

TABLE 3

Fatigue Strength Coefficients and
Exponents for Typical AWS Structural Welding Code
Fatigue Stress Categories for Redundant & Non-Redundant Structures^A

Redundant Structures

<u>Fatigue Category</u>	<u>Fatigue Coefficient, c</u>	<u>Fatigue Exponent, m^B</u>
A	3.77×10^{10}	-3.103
B	1.65×10^{11} *	-3.721
C	2.17×10^{10}	-3.478
D	4.53×10^9	-3.253
E	8.05×10^8	-2.897
		Mean -3.29

Non-Redundant Structures

A	2.88×10^{11}	-3.826
B	1.97×10^{10}	-3.340
C	1.58×10^{10}	-3.647
D	1.34×10^9	-3.083
E	8.34×10^7	-2.280
		Mean -3.24

^ADerived from AASHTO Standard Specifications for Highway Bridges (1992).

^BOverall mean slope for both redundant and non-redundant $N = f[S]$ fatigue categories is $m = -3.26$, excluding category F (welds in shear).

* If the fatigue exponent m for category is adjusted to $m = -3.26$, the fatigue coefficient is 2.47×10^{10} .

NOTE: Depending on the source of fatigue data, fatigue strength coefficients and exponents vary depending on the number of data points, scatter, and confidence level chosen. Numerous fatigue studies of hot rolled structural and low alloy steels and weldments have been completed by the Department of Defense, the Welding Institute (UK), the American Welding Society, the Society of Automotive Engineers, Lehigh University, and the University of Illinois. AASHTO/AWS fatigue data were used in this report due to its prevalent use in bridge design in the United States.

Using the multi-girder (redundant) Illinois Bridge 0160335 as an example, we can calculate the damage sustained by the bridge in one year. The critical detail instrumented for this bridge was a coverplate, and its stress-frequency histogram can be found in Figure 3. The $N = f(S)$ equation for a redundant cover plate (a category E detail) is $N = 8.05 \times 10^8 [S]^{-2.897}$. In the sample calculation of Table 4, the cumulative damage of both legal loads and permit loads are included. Permit loads are included, not only because of their significant damage, but also because under corrosive environments, even greater damage results to load-carrying members due to degraded surface conditions and sectional losses. These implications will be discussed subsequently, since corrosion and mechanical fatigue processes act conjointly on structural members.

The fatigue life of Illinois Bridge 0160335, per Table 4, is determined to be 86 years. This assumes no traffic growth, no changes in permit loads, and no corrosion of the principal main load-carrying members, and only for the fatigue of the cover plates. Other sections of the bridge may be affected by corrosion during the projected 86 years of cover plate fatigue life. These other sections subjected to corrosion may sustain higher stresses than the cover plates, which are typically located at points of counterflexure in continuous girders or at other locations where low stress ranges predominate.

TABLE 4

Calculation of Cumulative Damage
by Histogram - Linear Damage Method

No. of Stress Cycles/Yr.	Stress Range, ksi	Available Cycles, N_{sri}	n^i N_{sri}
1057596	1	8.05×10^8	.00131
368652	1.5	2.49×10^8	.00148
143592	2.0	1.08×10^8	.00133
41292	2.5	5.66×10^7	.00073
32736	3.0	3.34×10^7	.00098
23808	3.5	2.14×10^7	.00111
12276	4.0	1.45×10^7	.00085
12288	4.5	1.03×10^7	.00119
5580	5.0	7.60×10^6	.00073
2604	5.5	5.77×10^6	.00045
420	6.0	4.48×10^6	.00009
12	6.5	3.55×10^6	.00001
516	7.0	2.87×10^6	.00018
696	7.5	2.35×10^6	.00030
804	8.0	1.95×10^6	.00041
36	8.5	1.63×10^6	.00002
96	9.0	1.38×10^6	.00007
26	9.5	1.18×10^6	.00002
156	10.0	1.02×10^6	.00015
24	10.5	8.86×10^5	.00003
12	11.5	6.81×10^5	.00002
36	12.5	5.35×10^5	.00007
60	13.0	4.77×10^5	.00013
1,703,328 = N_t			.01166 = D

Notes: $N = 8.05 \times 10^8$ [S]^{-2.897}; histogram of Figure 3.
Life of structure = $1/D$; $1/(\.01166) = 85.8$ or 86 years

Effects of Corrosion on Fatigue of Steel

The general corrosion of plate steels used in various bridge components results in surface roughening and pitting. Crevice corrosion, another form of attack caused by oxygen deprivation, typically occurs when plates are bolted, riveted or are butted up against each other. Crevice corrosion can also result from the deposition of soil, dust, bird droppings or other debris on the steel. Typical load-carrying components that are affected by corrosion include wide flange beams, I-beam stringers, plate girders, diaphragm connections, floor beams, plates and gussets, and built-up sections consisting of riveted or bolted angles, channels and flat bars. Pins and eyebar linkages are also affected by pitting and crevice corrosion.

In uncorroded steels, the fatigue strength is that stress level below which the material can sustain an infinite number of stress cycles without failure. The fatigue strength of most carbon and alloy steels in air is approximately $0.5 \times$ [tensile strength]. However, when corroded, this proportion no longer holds, and fatigue strength is seriously degraded at high cycle fatigue.

Early studies of corrosion fatigue by McAdam² and Karpov³ show that surface roughening due to corrosion markedly reduced the fatigue strength of steels in high-cycle fatigue. In addition, the fatigue strength of corroded steels did not rise in direct proportion to tensile strength like those of polished steels in air, but largely remained constant like those of notched specimens.⁴ Surface roughness induced by corrosion actually consists of

microscopic notches that degrade fatigue life, with the sharpness of the pitting or corrosion roughening directly related to the extent of fatigue life reduction. Corrosion fatigue is also the result of corrosion processes which remove the benefits of cyclic work hardening. Work hardening impedes the formation of slip steps, which is one of the microstructural causes of fatigue.⁵ However, although corrosion only occurs during cycles of wetness, the pitting induced by corrosion results in permanent effects which are constant during dry periods when the bridge is cyclically loaded. The surface effects of machining vs. grinding on fatigue life in air are compared with corroded surfaces in fresh water and salt water for several structural steels in Table 5.

TABLE 5

Fatigue Strength of Common Structural Steels
in Rotating Bending at 2×10^6 Cycles or Greater

<u>Structural Steel</u>		<u>Fatigue Strength in ksi*</u>			
<u>Grade</u>	<u>No. of Cycles</u>	<u>In Air</u>		<u>In</u>	<u>In</u>
		<u>Ground</u>	<u>Machined</u>	<u>Fresh Water</u>	<u>Salt Water</u>
ASTM A36	2×10^6	26.0	23.0	19.0	14.5
ASTM A36	$10^7 - 10^8$	26.0	23.0	4.6	4.3
ASTM A588	2×10^6	31.5	27.3	21.0	15.8
ASTM A572	2×10^6	29.3	25.7	20.8	15.3
ASTM A514	2×10^6	49.5	41.8	23.1	15.7

Note: Values obtained in rotating bending; computed per ASM Metals Handbook, Vol. 1, Properties of Iron and Steel, 9th Edition, Fig. 7, p 671; also from P. Forrest, Fatigue of Metals, Pergamon, 1962.

*1 ksi = 6.895 MPa

More recent work by Albrecht, Shabshab, Li and Wright⁶ of the University of Maryland compared the fatigue life of corroded flanges with the weld fatigue categories of the AWS Structural Welding Code.⁷ The fatigue category A of this code is a wide flange in bending in the as-rolled condition that has no welded attachments, with only a mill scale surface condition. Albrecht, et. al.⁶ fatigued both carbon and weathering steels previously exposed to the elements and found that carbon steels suffered lesser reductions in their fatigue strength than weathering steels, as shown in Figures 4 and 5. Further investigation showed that the pits in weathering steel were sharper and deeper, particularly in areas where crevice corrosion under heavy soil deposits occurred. Lateral gussets are especially vulnerable.

Such creviced areas, because of their semi-continual wetness, can approach immersion or tidal conditions associated with steel in seawater, particularly if the bridge receives liberal applications of deicing salts. The presence of deep pits represents a general increase in the number of surface notch effects on the steel, shifting the entire stress versus number of cycles curve downward. The presence of pitting affects the fatigue strength at all stress cycle levels for fatigue lives greater than 10^4 cycles.

Albrecht, et. al.⁶, proposed a fatigue reduction factor directly related to pit depth. Steels were also differentiated between carbon and weathering steels in their study.

Two separate predictive equations were proposed for each type of steel:

$$K_p = 1.0 + 0.22d_{mm} \quad (\text{carbon steel, mm}) \quad [\text{Equation 3a}]$$

$$K_p = 1.0 + 0.00559 d_{mils} \quad (\text{ASTM A36 carbon steel, mils}) \quad [\text{Equation 3b}]$$

$$K_p = 1.0 + 0.40 d_{mm} \quad (\text{ASTM A588, 242 \& 514 weathering steels, mm}) \quad [\text{Equation 4a}]$$

$$K_p = 1.0 + 0.0102 d_{mils} \quad (\text{weathering steels, mils}) \quad [\text{Equation 4b}]$$

Where: K_p = fatigue reduction factor due to pitting

d_{mm} = avg. depth of pits, mm

d_{mils} = avg. depth of pits, mils

This equation establishes that pits of 9 mm (358 mils) depth in carbon steel and 5 mm (196 mils) depth in weathering steel will result in a fatigue strength reduction of 3.

This fatigue reduction data is plotted in contrast to AWS welding fatigue categories A through E in Figures 6a (carbon steel) and 6b (weathering steel).

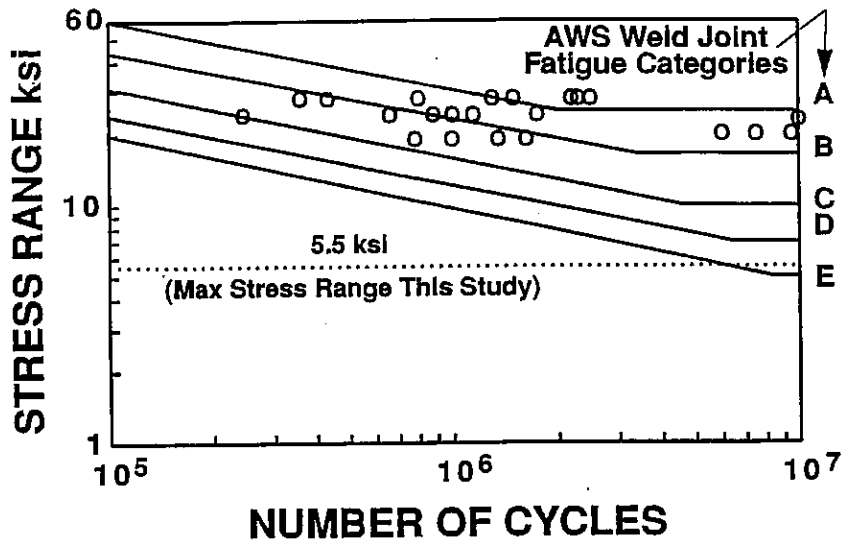
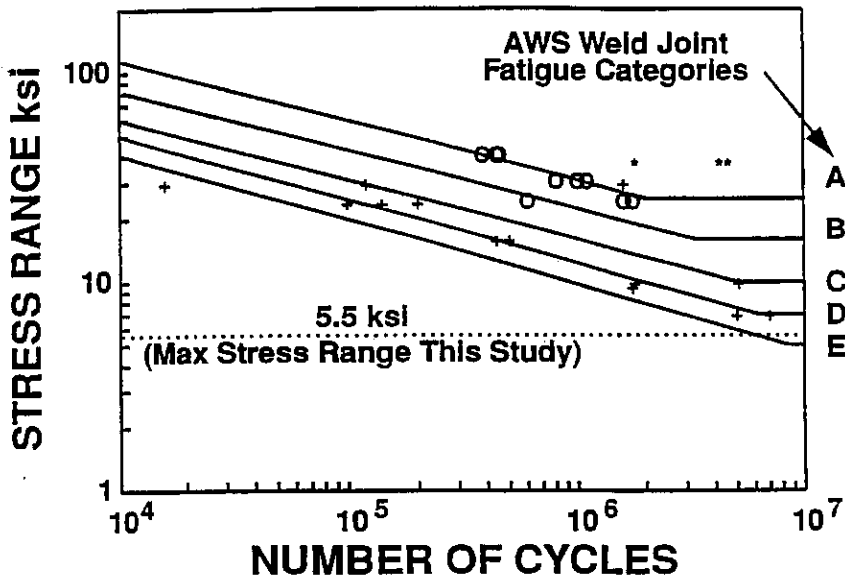


Figure 4. Fatigue test data for carbon steel beams (data of Albrecht, et al.).⁷



- + Sheltered Beams Tested in Moist Salt Water Env.
- O Boldly Exposed Beams Tested in Moist Fresh Water Env.
- * Boldly Exposed Beams Tested in Air

Figure 5. Fatigue test data for weathering steel beams (data of Albrecht, et al.).⁷

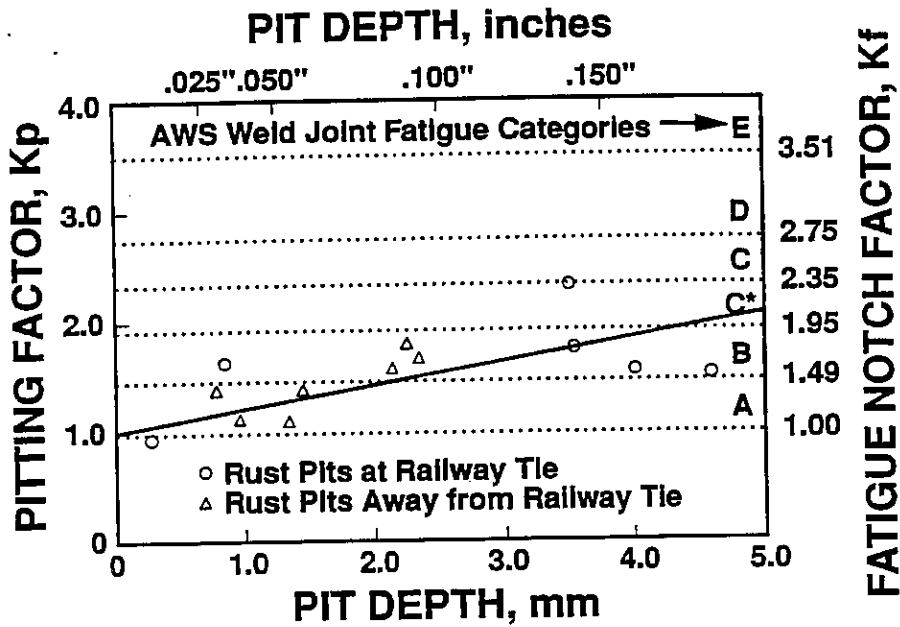


Figure 6a. Pitting Factor for carbon steel beams. Pits in plain carbon structural steel are generally rounded. Data of Albrecht, et. al.⁷

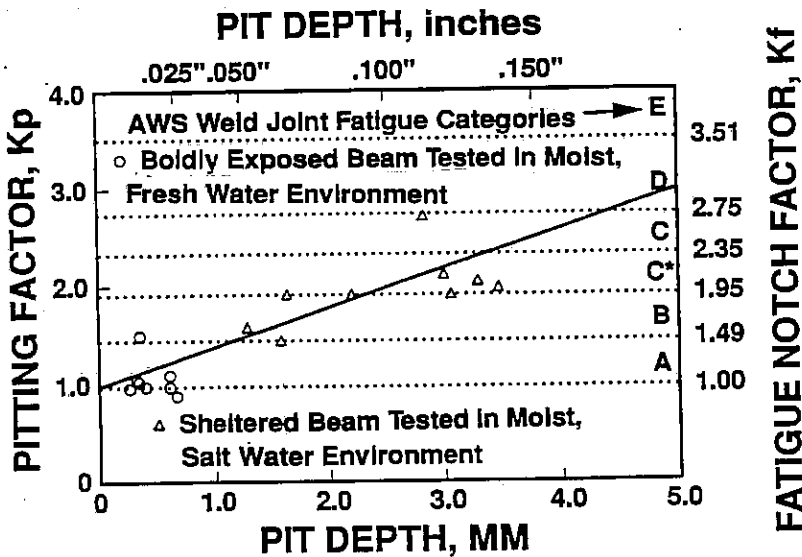


Figure 6b. Pitting Factor for ASTM A588 weathering steel beams. Pits in structural steels containing substantial levels of copper, phosphorus, and chromium are generally sharper than conventional structural steels. Data of Albrecht, et.al.⁷

Determining average pit depth for carbon and weathering steels is a means of adjustment of an appropriate fatigue category downward to conditions, using Category A as a baseline for uncorroded hot-rolled structural steel plate. However, there are two problems with this approach: (1) The fatigue category may not remain constant after the time of measurement if further corrosion occurs; and (2) the chemical composition range for ASTM A36 and ASTM A572 is so unrestrictive, particularly with respect to copper, chromium, and nickel additions, that they can behave as weathering steels. It is most evident in the Albrecht, et al.⁶ study that carbon and alloy steels have fatigue failure envelopes that are bounded between AWS Category A and Category D, as shown in Figures 4 and 5. A bridge of recent design may have structural members in Category A, whereas other bridges of advanced age and sustaining considerable corrosion are probably best characterized as Categories C or D.

The AWS fatigue categories give the impression that there is a fatigue limit at 2×10^6 cycles; however, other corrosion fatigue studies of carbon steel immersed in fresh and saline waters or specimens which collect their condensate have shown that their fatigue limits at $10^7 - 10^8$ cycles are 4.3 - 4.6 ksi (29.6 - 31.7 MPa). This implies that the downward sloping straight lines of the AWS/AASHTO stress vs number of cycles plots should be further extended downward and do not have an endurance limit shelf at 2×10^6 or 5×10^6

cycles as depicted in the AWS Structural Welding or AASHTO Bridge Code. An endurance limit represents fatigue conditions in air, but not when condensation or active corrosion is taking place on the steel. As shown in Figure 5, the corrosion fatigue envelope for weathering steels extends from Category A to Category D. Extension of the Category D line to 40,000,000 cycles puts fatigue strength at about 4.5 ksi, which corresponds to similar results of rotating bending tests performed by other investigators.

The available number of cycles for the liberal upper bound for a smooth plate or beam is Category A, whereas Category D is the conservative lower bound to compare cumulative damage, as shown in Figure 5. The general equation for a fatigue category line is:

$$N = C[S]^m \quad \text{[Equation 2]}$$

Where: N = available number of stress cycles before failure

C = fatigue coefficient

S = stress range, ksi

m = fatigue exponent

The $N = f(S)$ equation for fatigue Category D, (non-redundant) as established by purely mechanical fatigue for structural steel in air, is as follows:

$$N = 1.34 \times 10^9 [S]^{-3.083} \quad \text{[Equation 5]}$$

Using an exponent of -3.26 and a fatigue strength in seawater as 4.3 ksi at 2×10^7 cycles, the coefficient C then equals: $[2 \times 10^7]/(4.3)^{-3.26} = 2.32 \times 10^9$. This can yield the lower bound for the corrosion fatigue equation:

$$N = 2.32 \times 10^9 [S]^{-3.26} \quad \text{[Equation 6]}$$

The fatigue coefficient for category D of the welding code is slightly lower:

$$N = 1.34 \times 10^9 [S]^{-3.26} \quad \text{[Equation 7]}$$

which is the form that will be used in this study for predicting available cycles for a severely corroded structural member. The slope of $m = -3.26$ is used to unify the upper and lower bounds. For non-redundant welded structures suffering slight-to-moderate corrosion, Category B is the conservative upper bound:

$$N = 1.97 \times 10^{10} [S]^{-3.26} \quad \text{[Equation 8]}$$

Category B is appropriate for welded plate girders as a starting point. As corrosion proceeds, the fatigue category shifts downward gradually from category A for rolled sections or category B for welded plate girders until, in later stages of fatigue life, the smooth plate is heavily pitted and is then classified as Category D.

Further confirmation of this envelope is found in the work of Barsom and Rolfe,⁸ which shows a slope of -3.36 and a

narrow scatter band for four different structural steels immersed in a 3.5% chloride aqueous solution. In their work, [S] is expressed as $\Delta K/\sqrt{p}$, where ΔK is the change in stress intensity and \sqrt{p} is the square root of the notch radius. The notch radius is essentially equivalent to the pit radius. A summary of their work, along with many other investigations, is shown in Figure 7.

In this study, the effects of pitting on surface conditions and stress concentrations were studied, and the general effects of corrosion on the moment of inertia of structural shapes were directly quantified. These investigations were pursued in order to synthesize both corrosion and pitting rates and the AWS fatigue categories into a unified corrosion fatigue equation for structural steels. The AWS fatigue categories are used as reference markers only, and the corrosion fatigue equation represents the effect of corrosion and stress ranges, and not the notch severities or residual stresses that are associated with various weld details.

Corrosion of Structural Steels

Under various atmospheric and immersion conditions, plain carbon structural, weathering and high strength low alloy (HSLA) steels have different corrosion rates and susceptibility to pitting. When subjected to salt water immersion, weathering or copper-bearing steels have 21-65% greater corrosion and pitting rates than do ordinary plain carbon ASTM A36, SAE 1018 or SAE 1020 structural steels. The opposite is true for

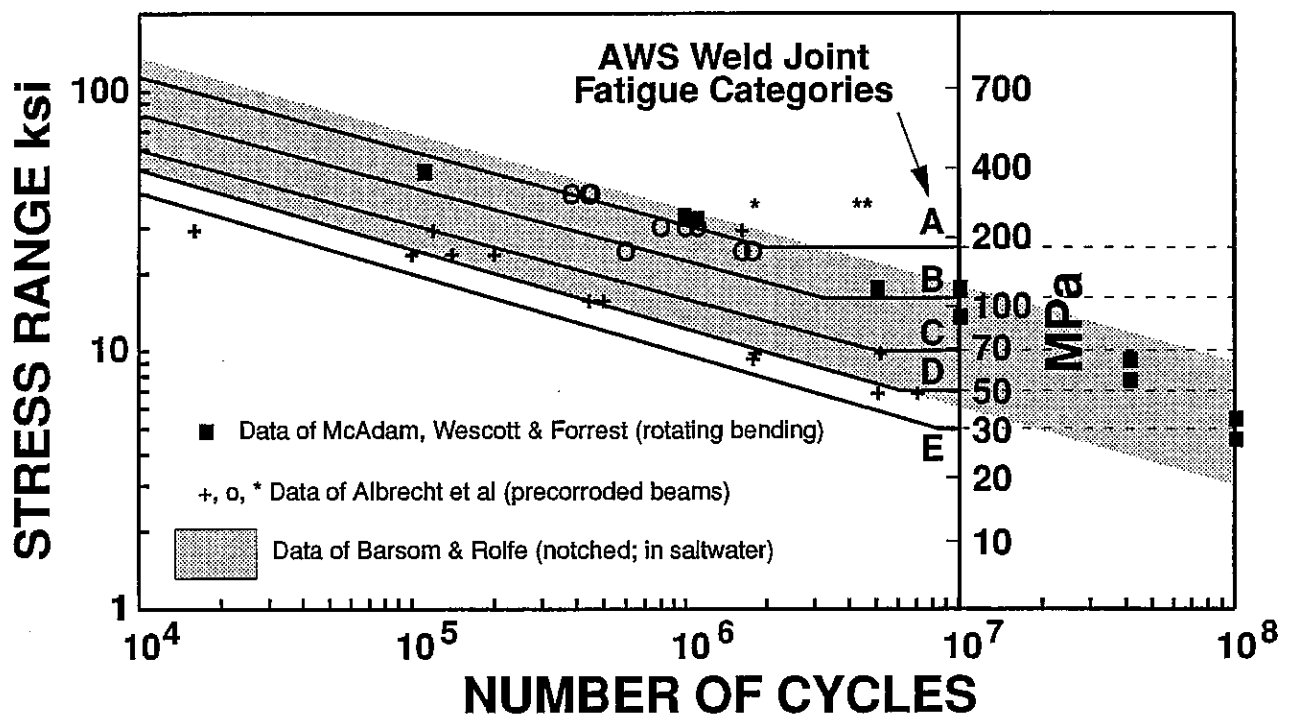


Figure 7. Plots of corrosion fatigue data of many investigators compared to AWS structural and weldment fatigue reference lines.

atmospheric exposures. The general corrosion performances in atmospheric and salt water immersion for a variety of bridge steels, including ASTM A36, A242, A588, and A514 are summarized in Table 6.

Several general trends emerge from the atmospheric and immersion test data for structural steels. First of all, the corrosion rate under immersion conditions is approximately 10 times the corrosion rate in the atmosphere. In addition, the distance from a large body of water to the bridge affects the amount of condensation and deposition of salt. As the distance to a large body of water from the bridge decreases, corrosion rates and pitting progressively increase. A similar analogy can be drawn for bridges which receive substantial and continuous applications of deicing salts.

For bridges located over rivers or streams, condensation can result in conditions similar to alternate tidal drying and wetting or direct immersion. Over a period of 50 years, substantial pitting and general corrosion can be sustained on many sites and locations throughout a bridge, particularly under deposits and crevices. Unless there are substantial climatic changes in the location, the average corrosion rate for structural steels over a long period of time is generally linear, as shown by various investigators.⁹ Pitting is proportional to corrosion rate, but the scatter of pit depth associated with a mean pitting rate is substantial. Nevertheless, overall trends indicate that average pitting rates

typically are approximately twice the general corrosion rate, ranging from 1.7 - 2.6, depending on the type of structural steel and its surrounding environment.

Effects of Corrosion on the Fatigue Failure Equation

Generalized corrosion, pitting, and the formation of deep crevices significantly affect the fatigue strength of structural steel. In various hot rolled structural steels containing substantial alloy additions of copper, sulfur, phosphorus, and chromium, the formation of deep, sharp pits can cause a severe reduction of fatigue strength at 10^7 cycles from 23 ksi (158 MPa) to 7 ksi (48 MPa) when corroded, according to the studies of Albrecht, et al.⁶

The fatigue failure equation, $N = C[S]^m$, is composed of three variables that are affected by corrosion. The exponent m is primarily related to the mechanical forces of crack propagation within the steel, with the corrosive environment causing small changes in the mean slope of -3.26 ± 0.50 . The approximate slope of these largely parallel lines of the various fatigue categories is $m = -3.26$.

TABLE 6

Corrosion and Pitting Rates of ASTM Structural Steels
in Various Environments*

<u>ASTM Structural Steel</u>	<u>Corrosion Rate, mpy^A</u>	<u>Pitting Rate, mpy^A</u>	<u>Pitting/Corrosion Ratio</u>
Intermittent immersion in saltwater			
A36	2.9	5.0	1.7
A588 Gr K	2.6	4.9	1.9
A595 Gr C**	2.6	5.9	2.2
A242	3.0	5.6	1.9
Immersion in saltwater			
A36	3.2	8.25	2.6
A588 Gr K	5.5	12.13	2.3
A595 Gr C**	5.4	10.0	1.8
A242	3.5	7.9	2.3
Temperate marine atmosphere, 800 ft (243m) from ocean			
A36	0.75	1.25	1.7
A242	0.33	0.59	1.8
A588	0.49	0.88	1.8
A514	0.39	0.78	2.0
Temperate marine atmosphere, 80 ft (24m) from ocean			
A36	16.3-20.0	22.7-33.4	2.0
A242	3.9	7.0	1.8
A588	7.9	14.2	1.8
A514	1.0	2.0	2.0
Industrial			
A36	0.34	0.57	1.7
A242	0.12	0.21	1.8
A588 Gr A	0.28	0.50	1.8
A514/517	0.14	0.28	2.0
Suburban and rural			
A36	0.30-.47	0.50-.79	1.7
A242	0.09-.14	0.16-.25	1.8
A588	0.20-.36	0.36-.65	1.9
A514	0.13-.16	0.26-.32	2.0

^A1 mpy = (in/yr) X (1000) = .0254 mm/yr

*Data based on 15.5 and 8-year exposures. Data presented are linear extrapolations beyond sampling times. Referenced from Corrosion of Metals in Marine Environments, Metals and Ceramics Information Center, MCIC Report 78-37, Columbus, Ohio, Tables 8, 21; Mar. 1978.

**An ASTM weathering steel grade used for tapered steel tubes used in luminaires and light poles.

Studies by Barsom and Rolfe⁸ of ASTM A36, A588, and A517 Grade F structural steels demonstrated that the slopes of $\Delta K / \sqrt{p}$ vs cycles to fatigue crack initiation were parallel and had an average slope of -3.36 when immersed and fatigued in a 3.5% sodium chloride solution. This indicates that corrosive conditions significantly alter the surface by creating fatigue notches, but that the crack propagation of cracks emanating from these notches under loading conditions at various frequencies is still an inverse cubic function. The other variable, C, is a function of corrosive environment and time, whereas S, stress range, is a function of loading, sectional area, and time. C is a surface-related function. If the surface is corroded and pitted, it decreases the amount of time before crack propagation can start. The Barsom and Rolfe⁸ studies reflect changes in ΔK by increasing applied stress. Their notch radius p is directly analogous to a sharp pit of considerable depth. Their studies, however, were conducted in a limited time frame. In actuality, bridges sustain corrosion damage slowly over a period of 50 years or more, gradually raising stress levels by pitting and section loss.

Since the surface conditions are being modified by corrosion, Category A or B fatigue strength changes as a function of time. Unlike laboratory fatigue studies where the ground or hot rolled surface remains intact, gradual changes induced by corrosion take place over the course of many years to alter fatigue strength in a bridge. In addition, the ambient stress state also increases as sectional losses are sustained,

assuming that present loadings remain the same. In many cases, traffic loadings may progressively increase. For wide flanges and I-beams, changes in moment of inertia due to corrosion losses in section also affect the ambient bending stress.

A general corrosion fatigue equation is proposed, taking general corrosion and pitting into account:

$$N = (C/K_f)[S_{corr}]^m \quad \text{[Equation 9]}$$

Where: N = number of available fatigue cycles at a given stress level

C = fatigue strength coefficient

S_{corr} = stress range in member, adjusted for moment of inertia or section loss due to corrosion

K_f = fatigue reduction factor, related to pitting

R = corrosion rate, mils per yr.

t = time, years

m = fatigue strength exponent, typically -3.26 for structural steels

If strain gages are used for the measurement of stresses in structural steels in the corroded critical sections, the term $[S_{corr}]$ is unnecessary since the strain gages reflect actual stress values. However, because of the difficulty of placing gages on corroded sections, use of stress concentration factors may be necessary.

In this investigation, the effects of surface attack, pitting penetration and section size were determined for actual corroded steels. This included the verification of the fatigue reduction factor K_f and the effects of section loss on the term $[S_{corr}]$.

STRESS CONCENTRATION AND FATIGUE STRENGTH

A structural member sustaining both surface pitting and section loss is subject to a phenomenon termed stress concentration due to significant geometrical changes. Surface pitting decreases the initiation time for fatigue cracks to form, whereas penetration by corrosion influences both local and overall gross stresses in structural members. Unfortunately, stress concentration effects are not easily divided by a sharp demarcation of surface pitting influences vs. predictable geometrical changes because corrosion itself is not entirely uniform. There may be sharp pits in one section, whereas there might be gradual section changes with shallow pits in an adjacent area of the structural member.

To verify the effects of pitting and section change on stress concentration, strain gages were actually mounted on corroded sections cut from steel plates that were removed from several older bridges. The plates were cut into coupon shapes and a 7/8" diameter hole was drilled on each end for load application in a universal tensile testing machine. The profiles of each specimen were measured with micrometer vernier calipers and pit depth indicators accurate to 0.001" (25.4 micrometers). The specimens varied in length, and were loaded to obtain a nominal stress of 1,000 psi (6.895 MPa) in their original cross sectional area. The general geometry of the specimens is shown in Figures 8 through 18.

After characterizing each specimen, a strain gage was mounted on the specimens in order to compare calculated nominal strain based on net section with actual strains where pits or section loss occurred. A typical strain gage working arrangement is shown in Figure 19. The strain was measured with foil strain gages at various locations on the specimen, particularly at pitted or penetrated areas, resulting in a stress concentration factor defined as follows:

$$K_f = \frac{\text{actual stress in corroded area}}{\text{nominal stress in corroded net section}} \quad [\text{Equation 10}]$$

The results of these tests are summarized in Table 7 which compares pit depth vs K_f and original specimen thickness/pit radius vs K_f . Pit radii were determined by the use of Intergraph Computer-Aided Drafting (CAD) systems.

The fatigue reduction factor K_f as a function of pit depth data exhibits wide scatter as shown in Figure 20, but is roughly linear and has a fair Pearson correlation coefficient of $r = +0.719$. A lower value correlation coefficient is to be expected, since pit depths vary widely in a specimen. The steels tested in this investigation either conform to ASTM A36 or ASTM A7 (an obsolete specification). For comparison, the fatigue reduction factor lines of Albrecht et al.⁶ are drawn. These lines represent plain carbon and weathering steels; weathering steels showing the severest reduction and plain carbon steels having the least reduction. The best fit

line of the strain gage data of this investigation lies right in-between the weathering and plain carbon steel lines of Albrecht and co-workers. The equation for the best fit line for strain gages is:

$$K_f = 1.2 + 5.77 [P] \quad \text{[Equation 11]}$$

Where: P = pit depth, inches
K_f = stress concentration

The deficiency in solely using pit depth alone as a predictor of strain concentration is that it does not take section changes, pit radius, and size effects into account. Theoretical studies of notches and grooves of plates in bending and tension have been extensively studied in the literature and are well summarized by Peterson¹⁰.

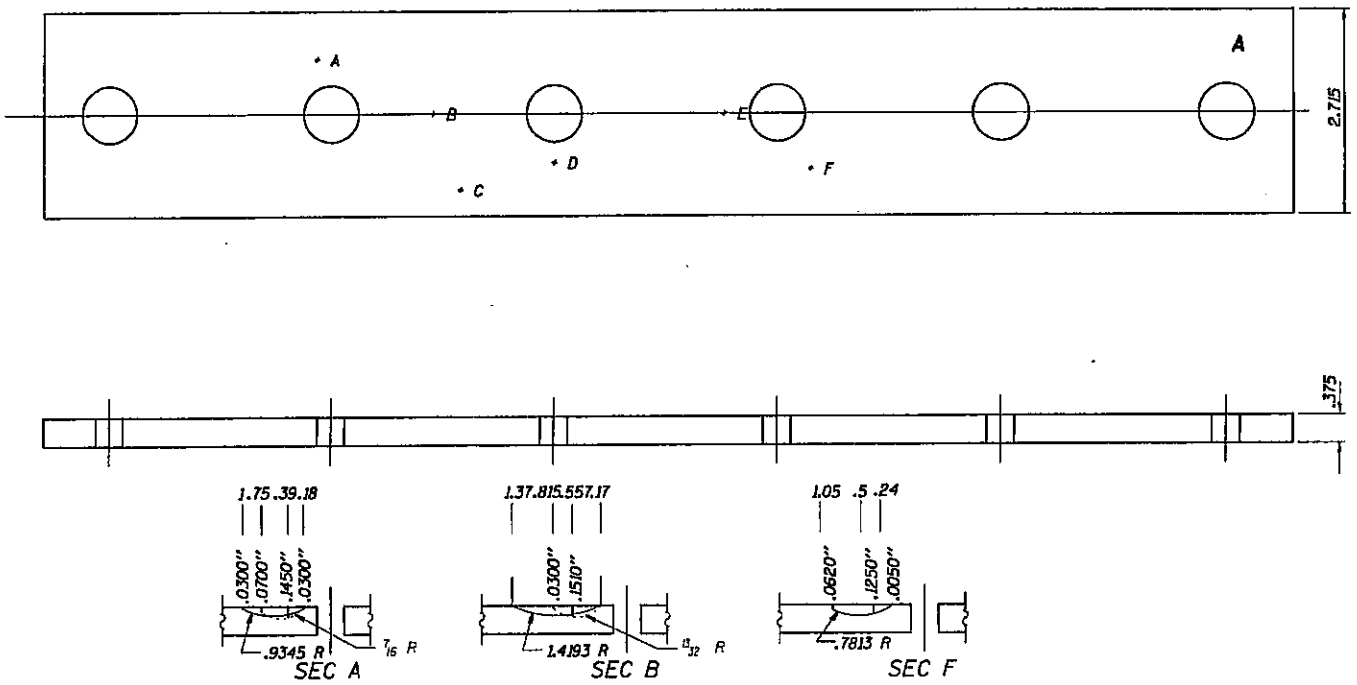


Figure 8. Dimensions and pitting in Specimen A. Scale = 0.39.

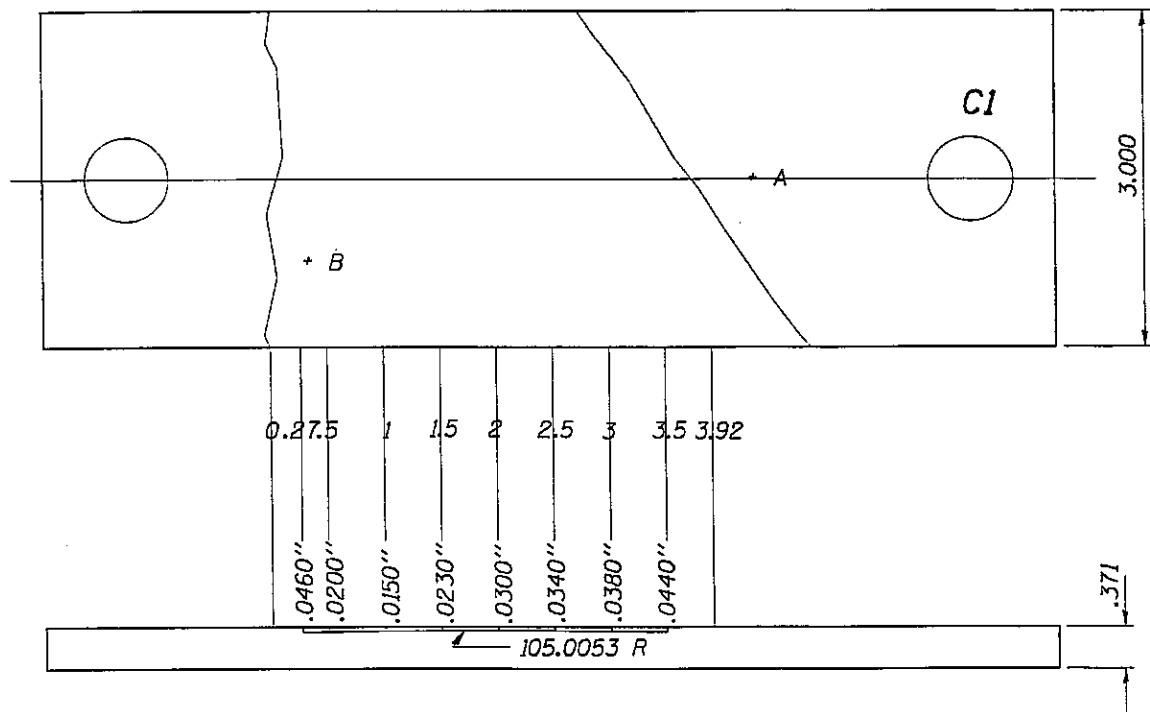


Figure 9. Dimensions and pitting in Specimen C1. Scale = 0.59.

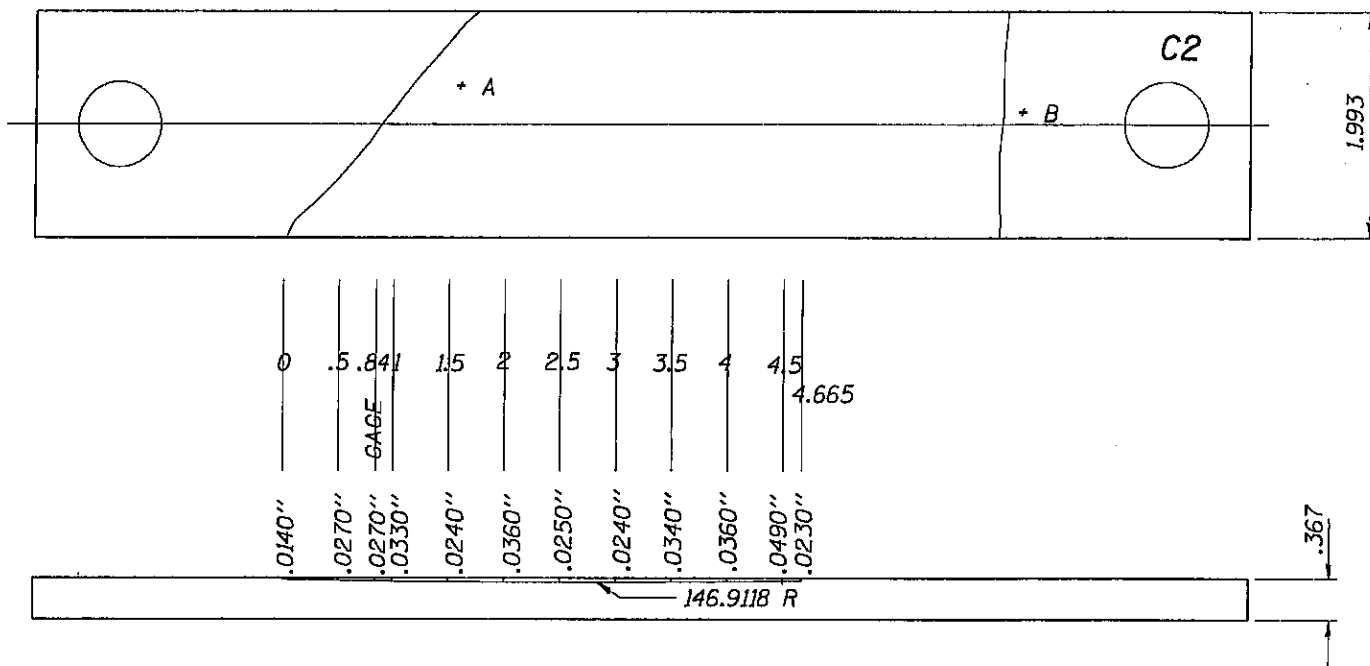


Figure 10. Dimensions and pitting in Specimen C2. Scale = 0.59.

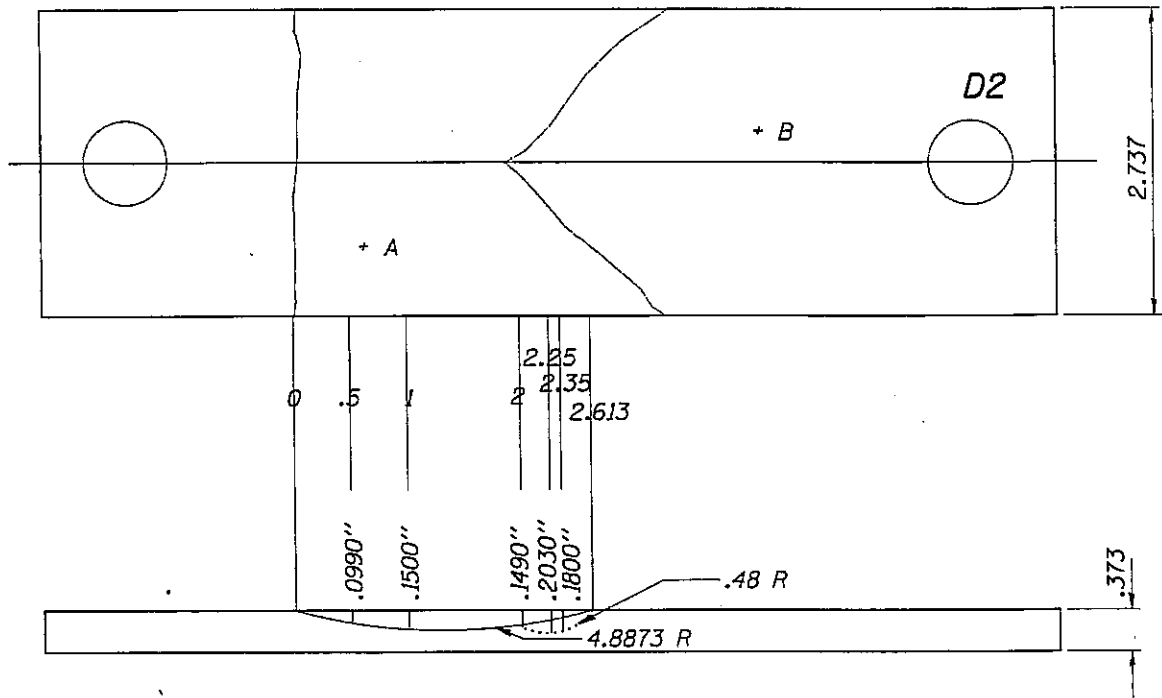


Figure 11. Dimensions and pitting in Specimen D2. Scale = 0.59.

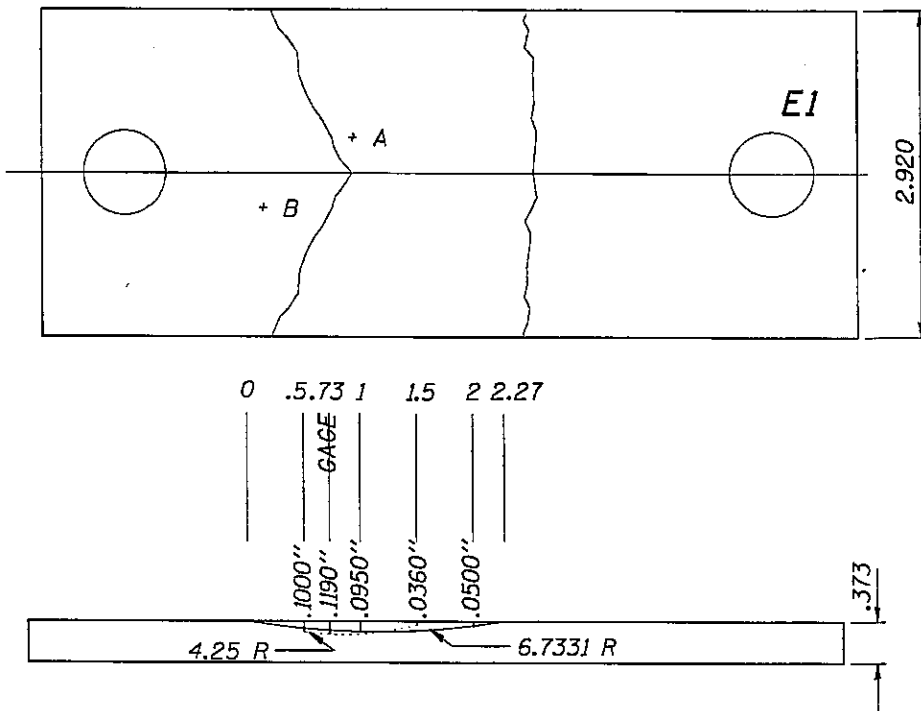


Figure 12. Dimensions and pitting in Specimen E1. Scale = 0.59.

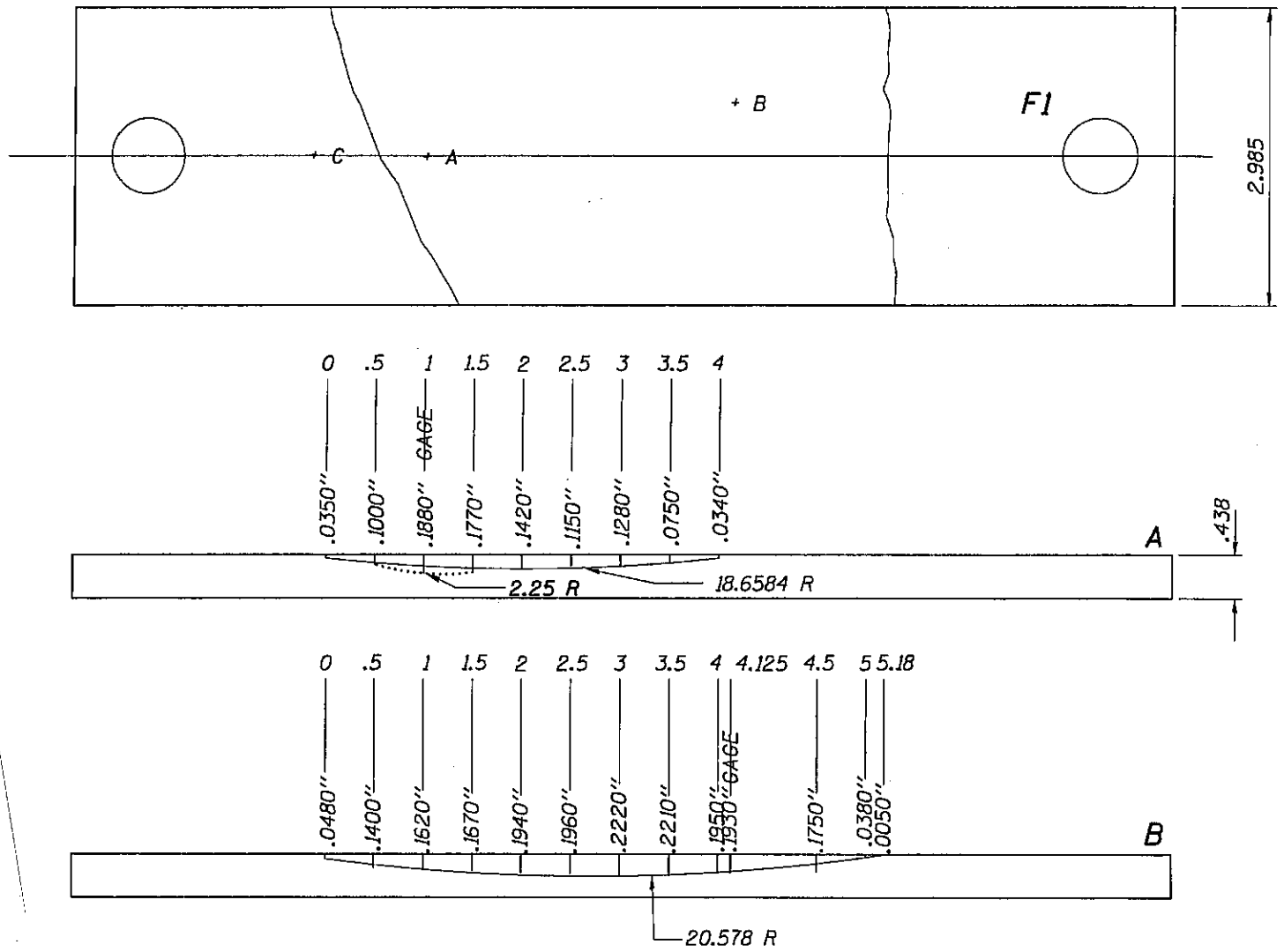


Figure 13. Dimensions and pitting in Specimen F1. Scale = 0.59.

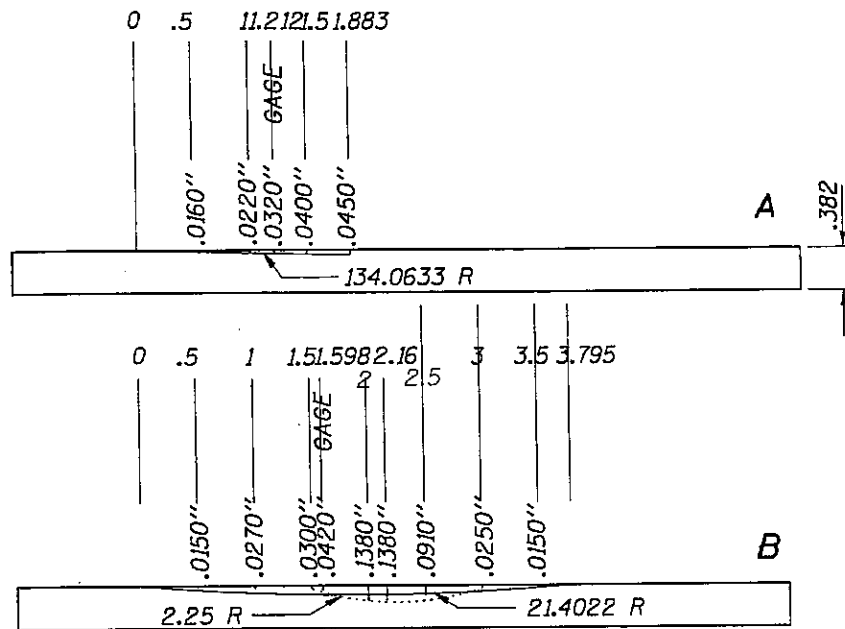
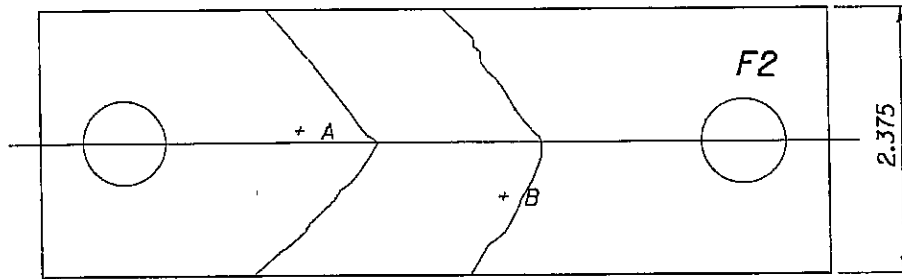


Figure 14. Dimensions and pitting in Specimen F2. Scale = 0.59.

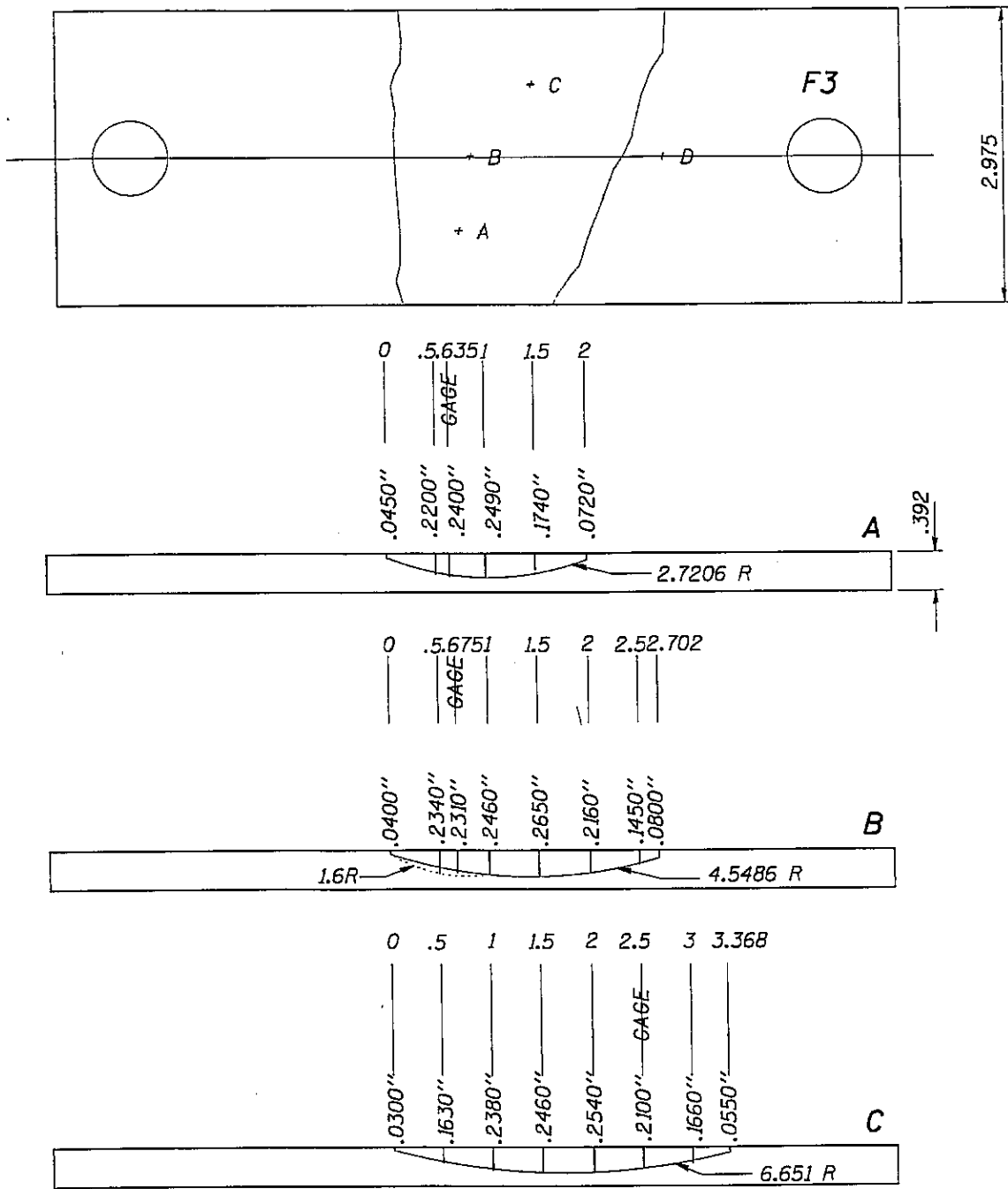


Figure 15. Dimensions and pitting in Specimen F3. Scale = 0.59.

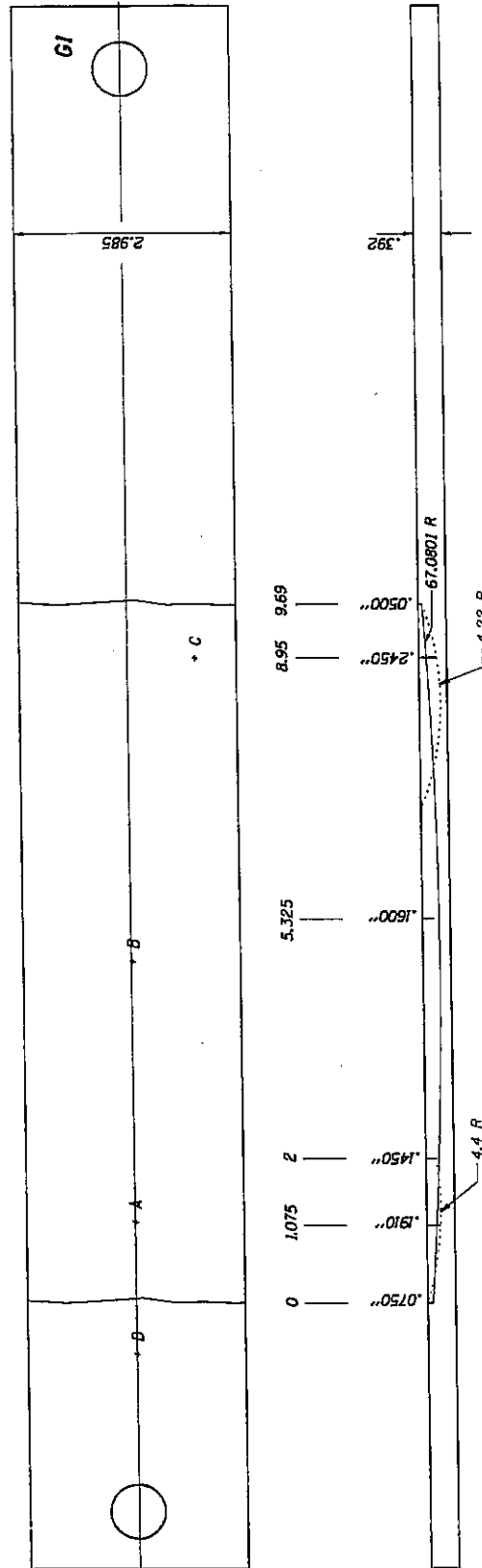


Figure 16. Dimensions and pitting in Specimen G1. Scale = 0.39.

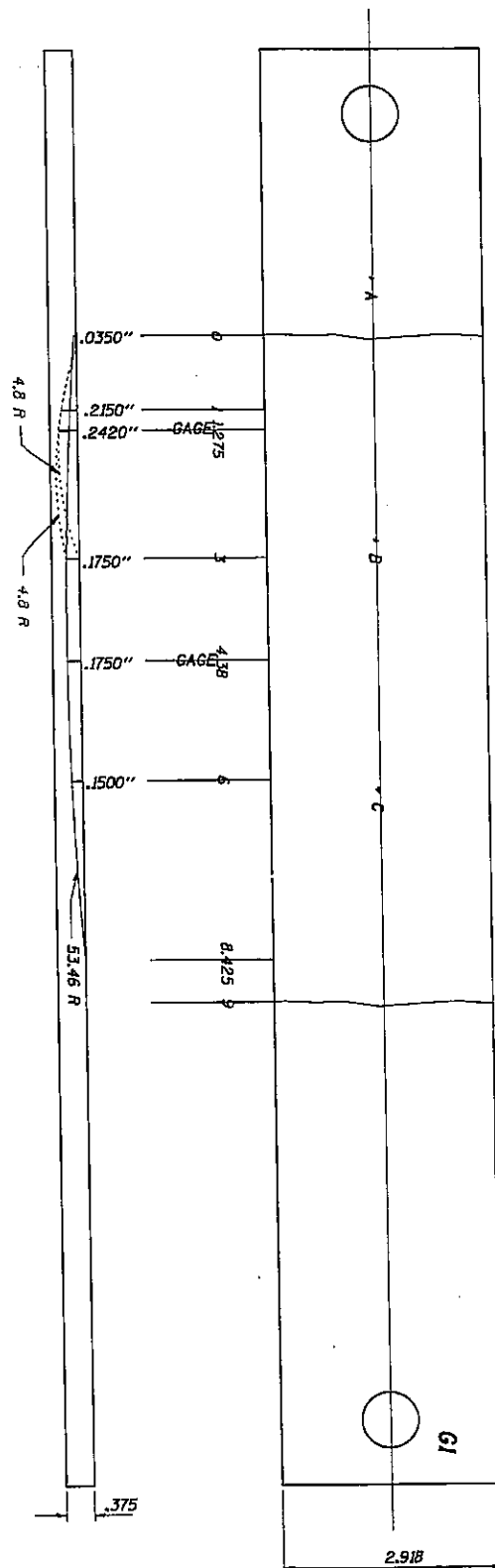


Figure 17. Dimensions and pitting in Specimen G1. Scale = 0.39.

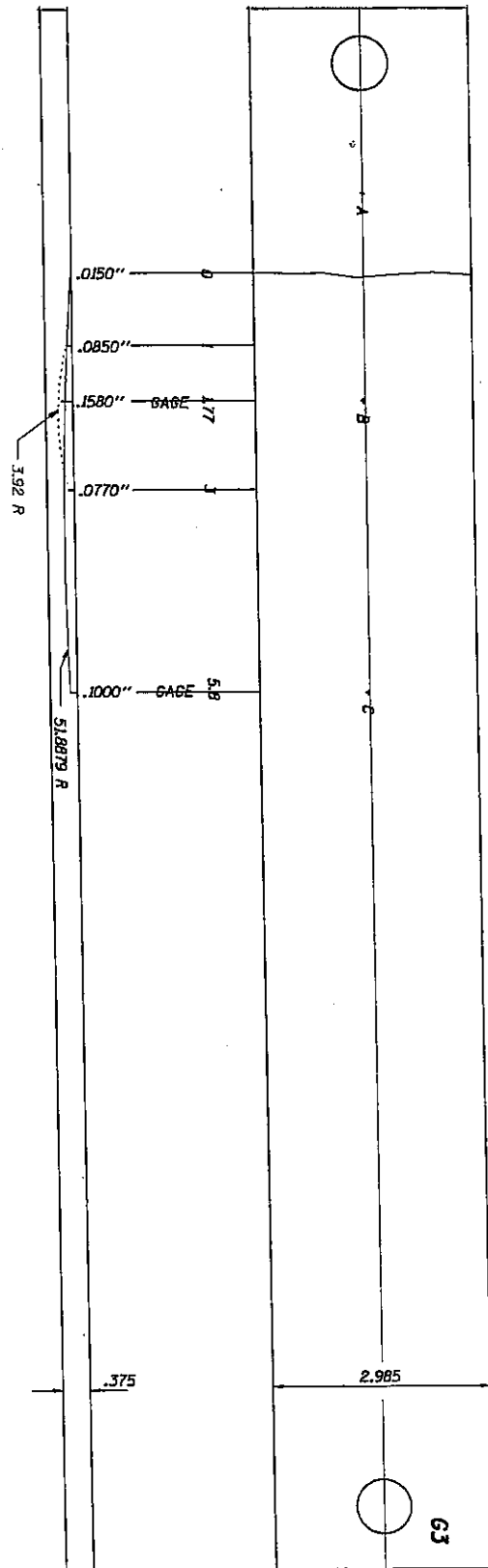


Figure 18. Dimensions and pitting in Specimen G3. Scale = 0.39.

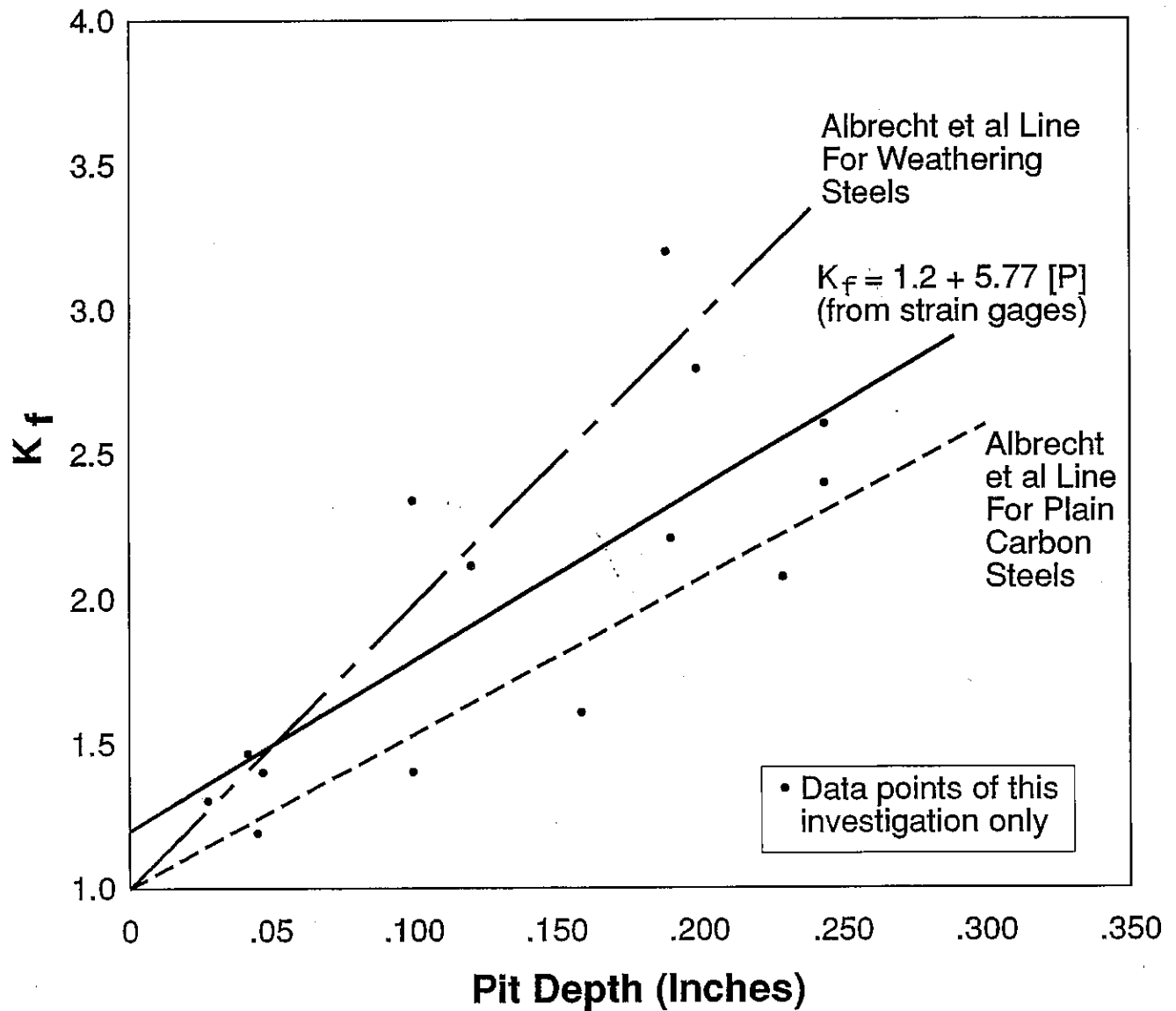


Figure 20. Stress concentrations derived from strain gage data plotted vs. the pit depths in the plate specimens.

The problem with using theoretical photo-elastic models as described in the literature is that they have uniform radii, defined spacings between notches and defined changes in section, namely because they are intended for design analysis of machined parts. Unfortunately, corroded components often have irregular changes in section, unequal pit depths, and non-uniformity in their groove spacing and irregular distribution in a plate or structural shape. The most common variables used in photo-elastic analyses of stress concentration are r_n , radius of the notch; D , the thickness or width of the plate; d , plate thickness separating grooves on opposite sides; and b , groove spacing, center to center.

In corrosion, with radius r_n becomes pit radius R_p . Groove spacing is extremely difficult to measure due to the randomness of corrosion. The variables of pit depth, plate thickness and pit radius (R_p) can be incorporated into the parameter D/R_p , since pit radius and pit depth are intimately related. A plot of $K_f = f(D/R_p)$ is shown in Figure 21. The function is well correlated ($r = + 0.776$), even in linear form, as follows:

$$K_f = 7.54 [D/R_p] + 1.53$$

Where: D = specimen or plate thickness

R_p = pit radius of curvature

K_f = strain concentration

This relationship is a better predictor of strain concentration than pit depth alone, which exhibits wider scatter.

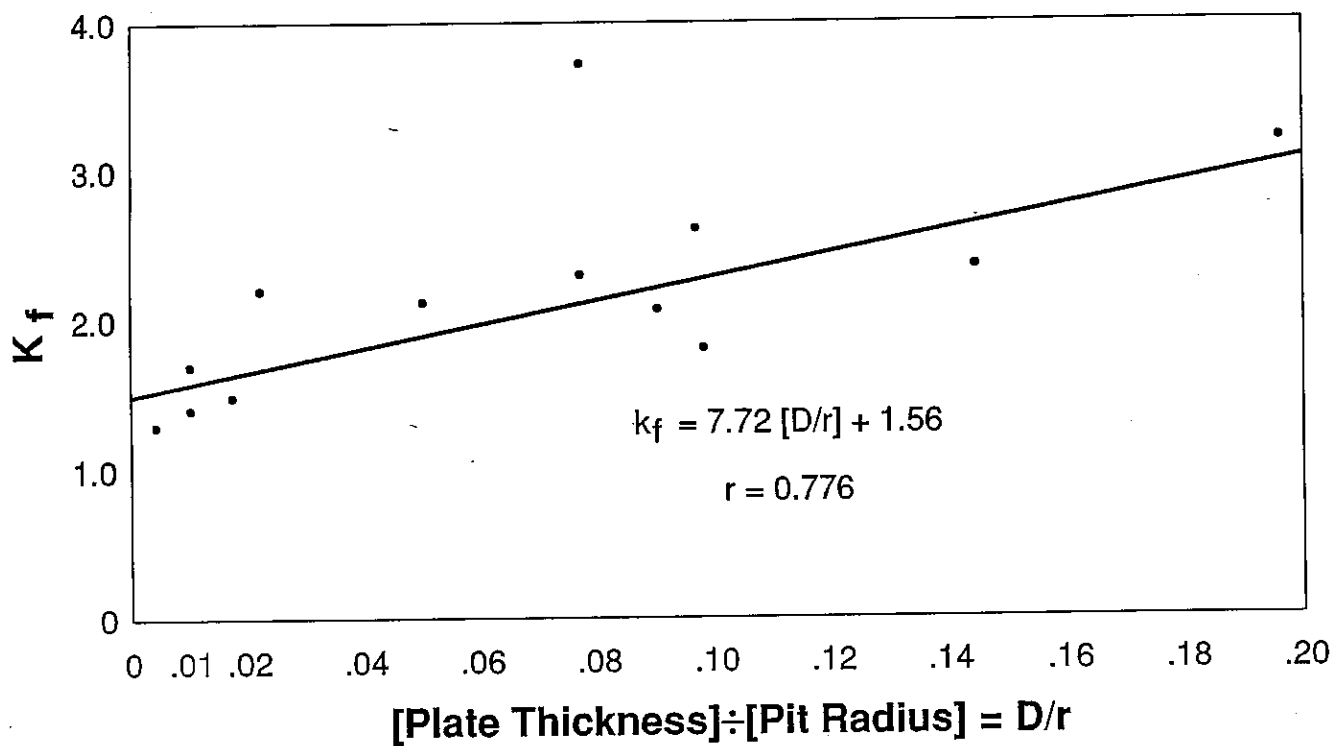


Figure 21. Stress concentration factor K_f in corroded plate specimens was derived from strain gage data, and plotted vs. the function of plate thickness divided by pit radius. The correlation coefficient, r , for this data plot is +0.776.

TABLE 7

Pit Depths, Radii, Specimen Thickness and
Stress Concentrations for
Instrumented Corroded Plates

<u>Pit or Penetration Depth (d)</u>	<u>Specimen</u>	<u>Radius(R)</u>	<u>Thickness(D)</u>	<u>D/R</u>	<u>dD/R</u>	<u>k_f</u>
0.245 inches	G1	4.2 inches	.367 inches	.093	.0228	2.60
.158	G3	3.92	.375	.096	.0152	1.59
.100	G3	52.0	.375	.007	.0007	1.41
.119	F3	6.7	.373	.056	.0067	2.13
.032	F2	134.0	.382	.003	.000096	1.33
.042	F2	21.4	.382	.018	.00076	1.46
.188	F1	2.25	.438	.195	.0367	3.22
.193	F1	20.5	.438	.021	.0041	2.18
.175	G2	53.5	.375	.007	.00123	1.73
.099	D2	4.9	.375	.077	.00762	2.33
.203	D2	4.9	.375	.077	.0156	2.78
.242	F3	2.7	.392	.145	.0351	2.37
.231	F3	4.5	.392	.087	.0201	2.07

1 inch = 2.54 cm

EFFECTS OF CORROSION ON THE MOMENT OF INERTIA

In order to measure the effects of corrosion on the moment of inertia of structural wide flanges, a loading test device was constructed to measure the deflections of corroded beams under uniform loads. Corroded steel I-beams, whose original dimensions corresponded to a standard 12 x 31.8 equivalent beam, were taken from stringers from a bridge approach undergoing rehabilitation. The corroded beams were originally installed in 1926 and removed in 1991, and had sustained considerable degradation, both in the flanges and webs. The rated moment of inertia of an uncorroded 12 x 35 beam is 227.0 in^4 ($9.449 \times 10^{-5} \text{ m}^4$).

Moment of Inertia by Deflection

The beams, which varied in length from 151.7 - 155.5 inches (3.84 - 3.95 m), were uniformly loaded with solid concrete blocks on simple supports. Each block weighed $31.7 \pm 0.71 \text{ lbs}$ ($14.4 \pm 0.32 \text{ kg}$). Blocks were placed contiguously along the corroded beam's length. The deflection of the corroded beams was then measured with electronic dial indicators accurate to $\pm 0.0005 \text{ inches}$ ($\pm 12.7 \text{ micrometers}$) at various positions, including the beam's midpoint. The dial indicators were mounted on a separate unloaded reference beam which was not affected by deflection of the concrete floor since both corroded beam and the reference beam are supported on the same two round steel bars. When the dial indicators were floor mounted, hysteresis

effects developed due to floor deflections. Each row of blocks corresponded to a uniform loading of 8.75 lbs/in (1.532 kN/m). Blocks were added progressively until 4 rows of blocks were stacked, resulting in a final loading of 35.0 lbs/in (6.125 kN/m). The test set up is shown in Figures 22, 23, and 24.

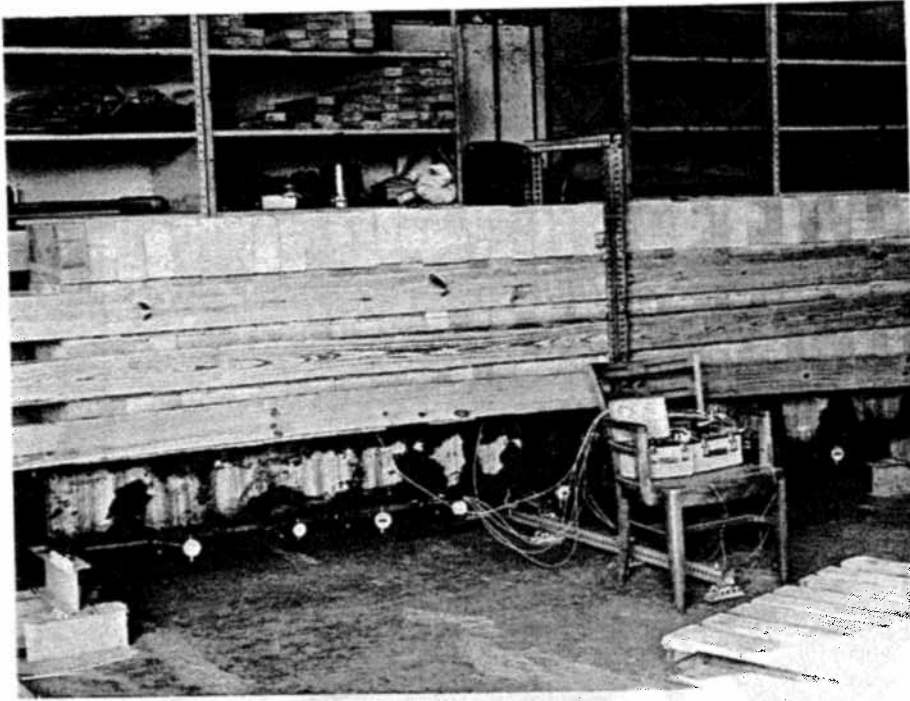


Figure 22. Overall view of deflection loading test frame set up. Deflections were measured at various distances along the beams, and cross-sectional measurements were taken at those same distances. This permitted a direct comparison of geometric measurements of moment of inertia with those moments of inertia calculated by deflection theory.

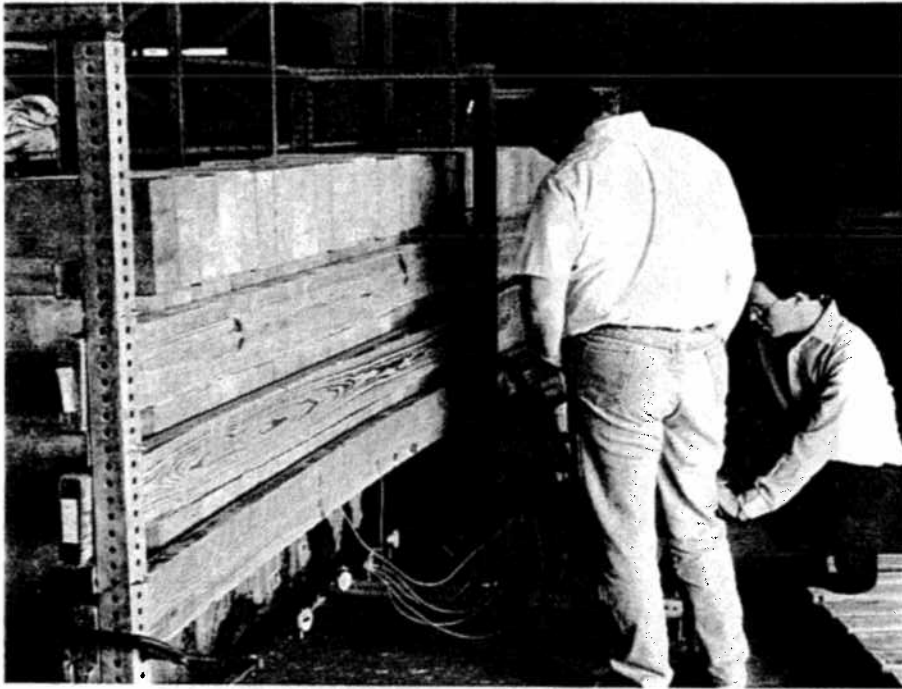


Figure 23. Strain gage readout of stresses to correlate with deflections measured by dial indicators accurate to 0.0001 inches (2.54 micrometers).

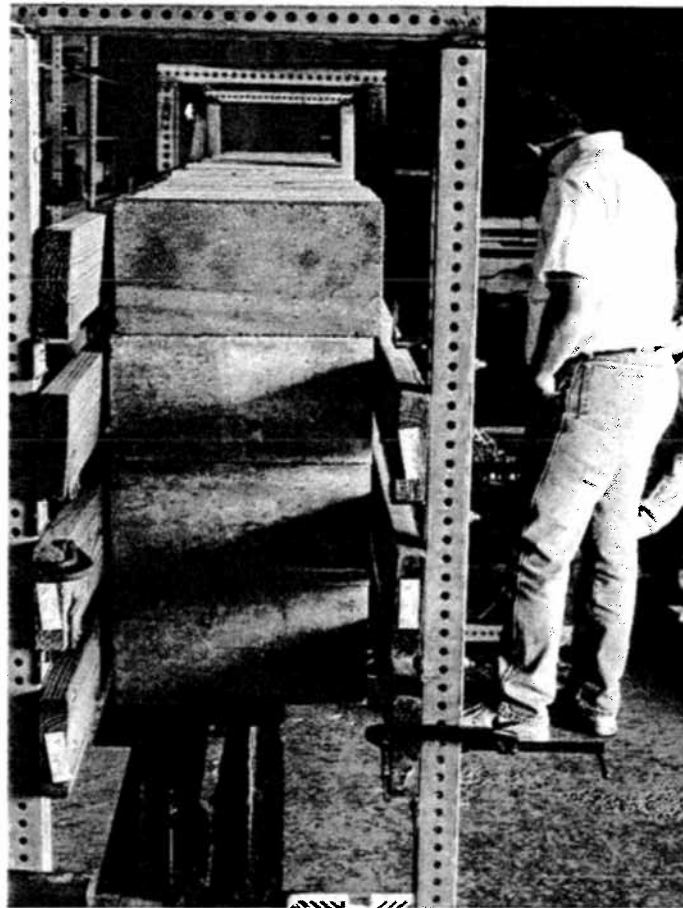


Figure 24. Frame restraints to prevent toppling of solid concrete blocks (uniform loading in 4 continuous rows). Final layer represents a uniform loading of a simply supported beam of 35 lbs/in (6.13 kN/m).

In order to calculate the moment of inertia by deflection, the classic elastic deflection equation for uniform loading on simple supports was used:

$$I = \frac{1}{24} \frac{Wx}{ELy} (L^3 - 2Lx^2 + x^3) \quad \text{[Equation 13]}$$

Where: I = moment of inertia, in^4

$W = wL$, where w = uniform loading/in = 35.0 lbs/in
 L = length of beam, inches

x = distance along beam from end supports, inches

y = deflection, inches

E = modulus of elasticity (for steel, 30×10^6 psi)

At midpoint ($1/2 L$), the moment of inertia is calculated by:

$$I = \frac{5}{384} \frac{WL^3}{Ey} \quad \text{[Equation 14]}$$

which is the simplification of the preceding deflection equation at $x = 1/2 L$. A summary of deflection data for beams 1, 2, and 3 can be found in Table 8.

The moment of inertia along a corroded beam is determined by incremental changes in the radius of curvature of a beam. Since the bending moment along the beam is determined in the test set-up by the fixed uniform loading, the moment of inertia can be precisely determined from the deflections at various points. The modulus of elasticity, for practical purposes of this test, was considered as constant throughout. All calculations assume a modulus of elasticity of 30×10^6 psi. Since the loading was not excessive, all deflections were elastic and, therefore, no permanent strain or deformation was recorded.

Moment of Inertia by Geometric Measurement

Although more complex measurements of the moment of inertia have been determined previously, a simplified technique was developed for field use and rapid calculation for rating purposes. This geometric measurement of moment of inertia was compared with the more accurate laboratory deflection measurements taken under uniform loading. The principle of measurement involves taking the average moment of inertia of a rectangular section, $I = bh^3/12$ and subtracting the internal void sections around the flanges and web. As schematically shown in Figure 25, the calculated moment of inertia is determined as follows:

$$I = I_t - I_1 - I_2 \quad \text{[Equation 15a]}$$

$$I_t = 0.083 \left[\frac{(W_t + W_b)}{2} \right] \left[\frac{h_1 + h_2}{2} \right]^3 \quad \text{[Equation 15b]}$$

$$I_1 = 0.083 \left[\frac{b_1 + b_2}{2} \right] [h_{m1}]^3 \quad \text{[Equation 15c]}$$

$$I_2 = 0.083 \left[\frac{b_3 + b_4}{2} \right] [h_{m2}]^3 \quad \text{[Equation 15d]}$$

Where: I = overall net moment of inertia, in ⁴

I_t = gross moment of inertia

I_1, I_2 = moments of inertia of the void sections

TABLE 8

Deflections of Corroded Beams* at 35 lbs/in Uniform Loading

<u>Beam Number</u>	<u>Length</u>	<u>Uniform Loading Distance from Support End</u>	<u>Deflection at 35 lbs/in</u>
1	151.69 inches	16.38 inches	.0195 in.
1	151.69	31.38	.0321
1	151.69	46.38	.0440
1	151.69	56.13	.0485
1	151.69	65.87	.0528
1	151.69	75.63 (midpoint)	.0545
1	151.69	86.19 (65.50)	.0530
1	151.69	96.75 (55)	.0509
1	151.69	111.75 (37)	.0367
1	151.69	132.75 (19)	.0250
2	157.38	24.00	.0290
2	157.38	42.63	.0465
2	157.38	54.00	.0517
2	157.38	65.63	.0575
2	157.38	72.50	.0582
2	157.38	78.63 (midpoint)	.0572
2	157.38	92.00 (65.38)	.0565
2	157.38	105.00 (52.38)	.0505
2	157.38	117.63 (39.76)	.0411
2	157.38	134.00 (23.38)	.0369
3	155.50	18.00	.0365
3	155.50	34.00	.0553
3	155.50	47.50	.0665
3	155.50	59.75	.0758
3	155.50	68.25	.0779
3	155.50	77.75 (midpoint)	.0812
3	155.50	93.50 (62)	.0750
3	155.50	104.25 (51.25)	.0780
3	155.50	114.75 (40.75)	.0585
3	155.50	135.25 (20.25)	.0335

*The corroded beams were originally 12 x 35 American Standard I-beams, whose dimensions are 12.00" deep x 5.078" wide x 0.428" web thickness.

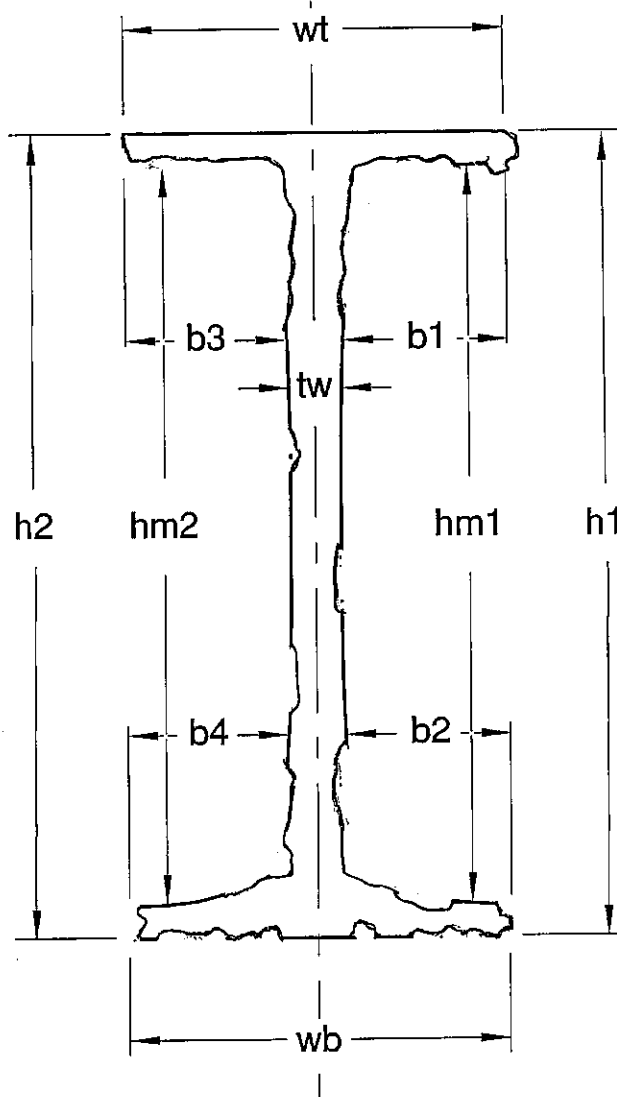


Figure 25. Basic measurements for determination of moment of inertia of wide flanges, I-beams or S-shapes. Measurements were taken with micrometer calipers. For measurements on a bridge where w_t is composite with the deck and the upper flange measurement cannot be made, the web thickness t_w should be made with an ultrasonic thickness detector and combined with $b_3 + b_1$. These measurements yield: $[b_3 + b_1 + t_w] = w_t$.

- w_t = width of top flange
- w_b = width of bottom flange
- h_1 = height of flange, side 1
- h_2 = height of flange, side 2
- b_1 = base width of top flange, side 1
- b_2 = base width of bottom flange, side 1
- b_3 = base width of top flange, side 2
- b_3 = base width of bottom flange, side 2
- h_m = mean height of void section, side 1
- h_{m2} = mean height of void section, side 2

These measurements were taken at various locations on the three deflected beams to correspond directly with the moments of inertia at those same points obtained by use of the elastic deflection equation. Measurements were obtained with instruments accurate to ± 0.001 inches (25.4 micrometers). These geometric measurements of the corroded beams taken at various locations are summarized in Table 9.

TABLE 9

Dimensions of Corroded Beams, Inches

<u>Beam #1</u>	<u>Overall Length Between Supports: 151.69"*</u>		
<u>Measurement</u>	<u>Location 1</u>	<u>Location 2</u>	<u>Location 3</u>
Length from support end, x	46.75	75.57	96.69 (55.00)
Mean height @ side 1, h_{m1}	11.054	11.148	11.174
Mean height @ side 2, h_{m2}	11.167	11.085	11.230
Mean base width (b_1 & b_2)	2.189	2.037	1.993
Mean base width (b_3 & b_4)	2.130	2.310	2.251
Outside height, h_1	11.797	11.779	11.777
Outside height, h_2	11.926	11.892	11.852
Bottom flange width, w_b	4.455	4.505	4.457
Top flange width, w_t	4.876	4.838	4.738

<u>Beam #2</u>	<u>Overall Length Between Supports: 157.38"</u>			
<u>Measurement</u>	<u>Location 1</u>	<u>Location 2</u>	<u>Location 3</u>	<u>Location 4</u>
Length from support end, x	42.63	65.63	78.63	117.62 (40)
Mean height, h_{m1}	11.088	11.155	11.133	11.100
Mean height, h_{m2}	11.461	11.120	11.274	11.129
Mean base width, (b_1 & b_2)/2	2.201	2.175	2.290	2.232
Mean base width, (b_3 & b_4)/2	2.248	2.260	2.328	2.314
Outside height, h_1	11.820	11.889	11.885	11.929
Outside height, h_2	11.858	11.947	11.979	12.003
Bottom flange width, w_b	4.715	4.695	4.755	4.773
Top flange width, w_t	4.740	4.835	4.825	4.895

<u>Beam #3</u>	<u>Overall Length Between Supports: 155.50"</u>				
<u>Measurement</u>	<u>Location 1</u>	<u>Location 2</u>	<u>Location 3</u>	<u>Location 4</u>	<u>Location 5</u>
Length from support end, x	47.25	60.00	77.75	93.25 (62.25)	114.5 (41.00)
Mean height, h_{m1}	11.304	11.281	11.198	11.310	11.134
Mean height, h_{m2}	11.346	11.272	11.248	11.210	11.203
Mean base width (b_1 & b_2)/2	1.981	2.239	2.261	2.228	2.238
Mean base width (b_3 & b_4)/2	2.066	1.464	2.058	2.210	2.249
Outside height, h_1	11.813	11.798	11.758	11.862	11.900
Outside height, h_2	11.916	11.632	11.810	11.886	11.959
Bottom flange width, w_b	3.535	3.966	4.070	4.519	4.689
Top flange width, w_t	4.768	3.677	4.863	4.892	4.874

*Beams only extended 1" beyond their supports on either side; distances in () are from the opposite support end. (1 inch = 2.54 cm.)

The moments of inertia determined by deflection measurements are considered to be the most accurate, whereas the geometric measurements are considered to be approximate. It is difficult to take into account all of the irregularities of corrosion by geometric measurements at various points. The moments of inertia determined by both deflection and geometric measurements are compared in Table 10, along with the percent error for the simplified geometric measurements. Geometric measurements of moment of inertia have a mean error of -2.0% below the defining deflection measurements. This is beneficial because it is preferable that geometric measurements be conservative. If a geometric measurement of moment of inertia is used on an active bridge, even more conservative estimates using only the least flange width, w , least outside height, h , and maximum mean inside height, h_m , can be used to insure a very safe minimum value for moment of inertia. This procedure is recommended if corrosion is severe. Severe corrosion involves web or flange perforation.

Geometric measurements are most easily accomplished by field personnel using accurate micrometers, calipers, and ultrasonic thickness detectors. Field deflection measurements are more difficult to obtain since beams are preloaded with deck weight and have load sharing effects when additional live or dead loads are applied to induce their deflections. Moreover, a separate unloaded reference beam must be established to determine the relative deflections at various points.

Beam deflection and mean geometric measurements yield similar results for moment of inertia when the sections along the beam are relatively uniform. When corrosion is concentrated in certain parts of the beam's web or flanges, the correlation is not perfect and error is introduced. Deflection measurements are related to changes of the radius of curvature and moment along the beam. If a short section of the beam is surrounded by sections suffering severe corrosion losses, its general deflection is influenced by its neighboring sections to a certain degree.

For beams where corrosion is severe, it is recommended that the least sectional measurement along the beam be the controlling dimension for the rated moment of inertia, immaterial of its location on the beam. For beams with relatively uniform attack, the moments of inertia measured at each location should be used for calculation of representative or rated stresses with respect to actual beam position.

TABLE 10

Moment of Inertia Obtained by Deflection Under
Uniform Load Vs. Mean Geometric Measurements, in⁴*

<u>Beam No.</u>	<u>Location</u>	<u>By Deflection</u>	<u>By Mean Geometry</u>	<u>% Error</u>
1	1	151 in ⁴	155 in ⁴	+2.6
1	2	148	148	0.0
1	3	144	138	-4.2
2	1	147	122	-17.0
2	2	151	161	+6.6
2	3	154	137	-11.0
2	4	163	170	+4.3
3	1	111	88	-20.7
3	2	111	70	-27.9
3	3	111	101	-9.0
3	4	114	129	+13.2
3	5	113	157	+38.9

Mean error -2.0%
Std. Dev. ± 7.6

* Note: To convert in⁴ to m⁴, multiply in⁴ by 4.16 x 10⁻⁷.

Effects of Atmospheric Corrosion and Deicers on Moment of Inertia

The moment of inertia of a structural member gradually changes as it corrodes in the atmosphere, or if it is intermittently subjected to solutions containing deicers such as calcium chloride or sodium chloride (rock salt). If a steel bridge is located in a suburban or rural location, its corrosion rate is significantly less than if spanning over a large river. Table 11 summarizes simplified corrosion rates and pitting rates for common structural steels used in Illinois and similar locations in the United States.

These overall corrosion rates can be applied to determine the changes in moment of inertia. The pitting rates, which are approximately 2 x [corrosion rate], can be used to determine their effects on fatigue life. A wide flange generally sustains relatively uniform corrosion, except during its last stages of attack when the web-flange interface corrodes away and the web is beset by various perforations. If the bridge deck is deiced, the top flange may also suffer corrosive attack, in addition to the webs and lower flanges. In order to calculate the effects of corrosion on the moment of inertia, the appropriate corrosion rate must be determined either by estimation from Table 11 or by actual measurement or observation. The uncorroded moment of inertia of a rolled wide flange or a plate girder as described in Figure 25 can be approximated by:

$$I_i = \frac{BH^3 - bh^3}{12} \quad \text{[Equation 16]}$$

Where: H = overall beam depth
 B = overall beam width
 $b = B - t_w$
 $h = H - 2(t_f)$
 t_w = thickness of web
 t_f = thickness of flange
 I_i = initial moment of inertia, uncorroded

The moment of inertia of a flanged beam after sustaining corrosion for many years can also be approximated by the following expression:

[Equation 17]

$$I_C = \frac{(B - 2Rt)(H - 2Rt)^3 - (B - t_w)(H - 2t_f + 2Rt)^3}{12}$$

Where: I_C = moment of inertia after 12 corrosion
 B = original width of flange, inches
 H = original depth of beam, inches
 R = corrosion rate of the steel, depending on location of the bridge
 t = time, years in the unpainted (rusted) state
 t_f = thickness of flange
 t_w = 1, 2 thickness of web

TABLE 11

Corrosion and Pitting Rates of Bridge Steels in
the Atmosphere and Deicing Fluids for
Unpainted Steels

<u>Location</u>	<u>ASTM Grade</u>	<u>Corrosion Rate in/yr***</u>	<u>Pitting Rate in/yr***</u>
Rural atmosphere	A36*	0.00030	0.00050
Rural atmosphere	A588**	0.00020	0.00036
Suburban atmosphere	A36*	0.00047	0.00079
Suburban atmosphere	A588**	0.00036	0.00065
Industrial atmosphere	A36*	0.00034	0.00057
Industrial atmosphere	A588**	0.00028	0.00050
Creek or river crossing	A36*	0.00075	0.00125
Creek or river crossing	A588**	0.00049	0.00088
Intermittent deicing, but not over water	A36*	0.00290	0.00500
Intermittent deicing, but not over water	A588*	0.00260	0.00490
Frequent deicing, river crossing	A36*	0.00320	0.00825
Frequent deicing, river crossing	A588**	0.00550	0.01213

*Note: The corrosion rates for other plain carbon steels formerly used in structural work, such as ASTM A7 or SAE 1018/1020, are similar to ASTM A36.

**Note: Other weathering steel grades, such as ASTM A242, A595 Grade C, and some heats of ASTM A572 and A514 will have similar corrosion and pitting rates to ASTM A588, depending on composition.

***Note: 1 inch = 25,400 micro meters.

Extensive studies^{9, 11} of corrosion of metals and alloys have shown that after long periods of time, the overall penetration rates generally become linear functions after initial higher penetrations sustained in the first two years of exposure. This permits the use of a linear corrosion rate, R, in inches/yr, to be multiplied by time periods of 50 years or greater for thick sections.

The 12 x 35 standard I beams removed from the Shippingsport Bridge over the Illinois River are an example. These beams were subjected to frequent deicing during their lifetime of 65 years. The bridge was rusted and unpainted for periods totalling about 25 years.* A corrosion rate of 0.0032 in/yr is therefore chosen, reflecting the bridge's location as a deiced river crossing. The deflection measurements provided a range for moment of inertia between 111 - 163 in⁴, and geometric measurements provided a range from 70 - 170 in⁴. These variances reflect the statistical nature of corrosion and the non-uniformity of exposure and condensation associated with geometries inherent to bridge design and construction. The dimensions of a 12 x 35 standard beam before and after 25 years of uniform corrosion at 0.0035 in/yr are shown in Figure 26.

*NOTE: The bridge was painted in 1929, 1938, 1945, and 1972 and presently remains unpainted. Most bridge paints last approximately 7 years before significantly rusting. The bridge remained unpainted between 1952-1972 and between 1979 to present.

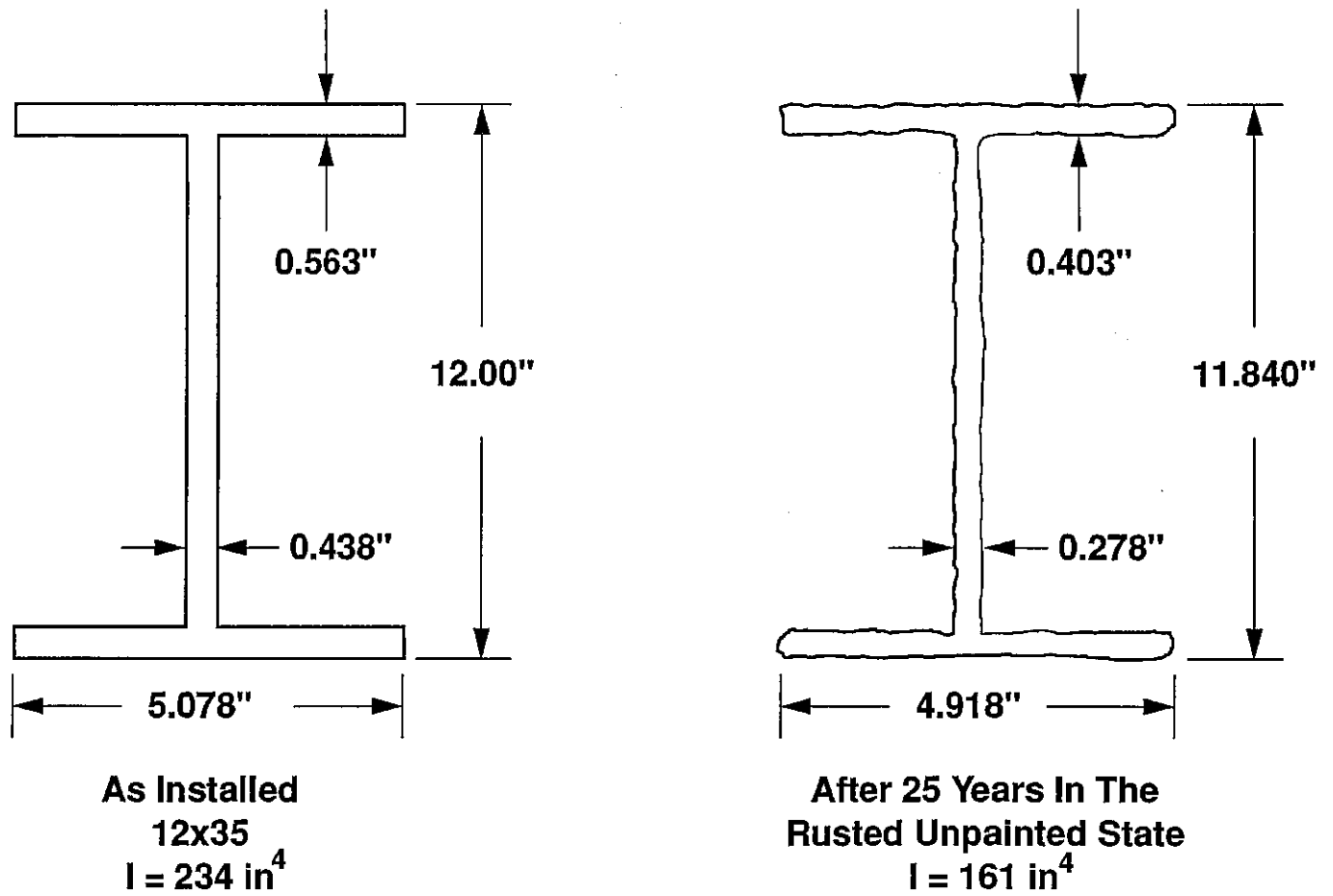


Figure 26. Effects of corrosion on a 12 x 35 standard I beam exposed to deicers. The bridge spanned the Illinois River for 25 years in the rusted unpainted state. Actual corrosion rate was determined to be 0.0035 in/yr.

After being left in the unpainted rusted state for a total of 25 years throughout its 65-year life, the 12 x 35 beam's original moment of inertia was degraded from an initial 235 in^4 down to an estimated 161 in^4 . This is in line with the ranges found by deflection, although it is evident that corrosion was not uniform at every beam, and corrosion rates probably varied between 0.003 to 0.004 in/yr. Such variation is typical for carbon steels in areas near a large body of water, which are subject to frequent condensation.

Further confirmation of the overall corrosion rate of 0.0032 inches/year was found by discovery of a rivet dropped onto a pier during the original construction of the bridge in 1926. The rivet had remained on a pier until discovered in 1991. A photograph of the rivet, including the rigid exfoliation corrosion products, are shown in Figure 27. The mean diameter of the rivet was 0.424 inches, which means that the original 0.875" diameter lost 0.226 inches per side. Over 65 years, this results in a corrosion rate of 0.0035 in/yr, which is a 9% difference vs. the table value of 0.0032 in/yr. The pier caps were degraded because of seepage of deicing salts and the continual freeze/thaw. The rivet sustained similar exposures that the standard 12 x 35 I beams also experienced, except that bridge deck undersides are often subjected to continuous condensation. Continuous condensation, coupled with deicers diffusing through the porous concrete deck, can result in conditions nearly equivalent to placing the beams under saline immersion.

Using the corrosion rate of 0.0035 in/yr from the bolt, the calculated moment of inertia is 154 in^4 , which is very comparable to the actually measured moments of inertia for beams 1 and 2 extracted from the bridge. Beams 1 and 2 exhibited uniform corrosion, whereas beam #3 exhibited substantial variations in section separated by distances as small as 5" - 6" (13 - 15 cm). The mean moment of inertia by deflection for beams 1 and 2 was 151 in^4 , whereas the mean moment of inertia for beam #3 (severely corroded) was 112 in^4 . The estimated corrosion rate for beam #3 is 0.0048 in/yr.

Effects of Pitting Rates on the Fatigue Characteristics of Structural Shapes

Various structural steels have different corrosion rates with respect to their environmental, exposure, temperature, and chemical composition of the steel. The corrosion rate markedly varies with environment and exposure to various salts. In general, the corrosion rate of unalloyed structural steels like ASTM A36 is about twice that of weathering steels in rural, suburban, or industrial atmospheres. If weathering steels are completely immersed or intermittently immersed in aqueous chloride solutions, their advantage over conventional ASTM A36 structural steels disappears. Under such conditions, weathering steel may actually have higher corrosion rates. In spite of the variation of corrosion rate for these various steels with environment, the ratio of average pit depth to overall corrosion rate varies

between 1.7 - 2.6, as shown in Table 11. The mean value for the pit ratio of depth to corrosion rate for all exposures of ASTM A36, A242, A588, and A514 steel is 1.9 ± 0.22 . Considering the statistical nature of corrosion, a close approximation of the (pitting rate for steels)/(overall corrosion rate) = 2.0.

Using published atmospheric corrosion rates for various steels, the fatigue reduction can be estimated by using the pitting factor of $2.0 \times$ [corrosion rate]. If a more accurate measure of fatigue reduction is desired, the pit radii should be measured in vulnerable sections. The expression for determination of fatigue reduction factor as a function of pit depth is as follows:

$$K_f = 1.2 + 5.77 [p] \quad \text{[Equation 18]}$$

Where: K_f = fatigue reduction factor
[p] = pit depth, inches

or expressed as a corrosion rate,

$$K_f = 1.2 + 11.54[Rt] \quad \text{[Equation 19]}$$

Where: R = corrosion rate, inches/yr
t = time, years

EFFECTS OF CORROSION ON THE LOAD-CARRYING CAPACITY OF REBARS

Reinforcing bars are the principal load-carrying members by design in reinforced concrete used in bridge decks or other reinforced structural members such as piers or abutments. If the concrete is sound and the bars are uncorroded, the reinforced concrete acts as a composite entity. However, if the bar is corroded, the bond between concrete and steel also dissipates and the low tensile strength of concrete results in cracking and

degradation of the structural element. Instead of sharing loads with the concrete, the reinforcing bars begin to entirely carry loads at cracks or where the bars have completely disbonded from the concrete matrix. Such bars are then subject to corrosion fatigue in the same way as are structural shapes and plates.

In this investigation, corroded and uncorroded reinforcing bars were removed from the deck approaches of the Shippingsport Vertical Lift Bridge over the Illinois River as were the standard I beams. The various bars were cut into varying lengths from 10" to 22" (25 to 56 cm), and then characterized with respect to depth of pitting, weight loss, and chemical composition. The bars were then subjected to mechanical testing to determine their tensile strength, yield strength and percent elongation. These mechanical properties were determined conventionally by noting the elastic and plastic behavior of the engineering stress-strain curves for each bar.

Depth of Pitting and Weight Loss

Even though bars may only suffer slight weight losses, the pitting sustained by the bars is considerably greater, markedly reducing their load-carrying capacity. Because reinforcing bars have a diamond-shaped deformation pattern, they inherently have natural crevices for pits to form and grow. Reinforcing bars are hot-rolled products, and have considerable mill scale and are rough-surfaced. Although a rough surface is beneficial for bonding to concrete, it constitutes a predisposed surface condition for corrosion and pitting. Without their concrete cover, rough corroded bars have markedly reduced fatigue strength.

In Table 12 the percent weight losses and the maximum pit depths for the various bars that were examined are summarized. The unit weight per inch for each bar was determined by weighing uncorroded bars before and after a tensile test. The mean unit weight per inch before the tensile test for uncorroded bars was $25.27 \pm .25$ g/in (9.95g/cm), and was $25.03 \pm .26$ g/in. (9.85 g/cm) for bars subjected to a tensile test. During a tensile test, the bars lose tenacious scale and corrosion and the value of 25.03 g/inch was therefore used to compare weight losses of corroded bars after their tensile tests with bars that had sustained little or negligible corrosion losses.

A plot of pit depths vs weight losses in corroded bars not only shows wide scatter, but also demonstrates the substantial effects of even minor weight losses. Assuming the pit radius to be $2 \times$ [pit depth], stress concentrations in bars are severely magnified by only minor corrosion losses. For a bar sustaining a 5% weight loss, this corresponds to a pit depth of .042 inches (1.07 mm), and a radius of .084 inches (2.13 mm). Using the stress concentration factors developed by Moore and Jordan as described by Peterson¹⁰, this results in a K_t of 1.45. If the pit is on one side, as is usually the case, the K_t is 1.9 per the data of Cole and Brown¹⁰ for a bar with a circular notch on one side. Instead of using approximate theoretical solutions, the yield strengths of the corroded vs uncorroded bars were actually compared. In this method, % weight loss can be used to not only predict section loss, but also the elastic stress concentrations causing yielding.

Mechanical Properties Predicted by Composition

Since the bars had slightly different compositions, their predicted yielded strengths from composition were compared and normalized with actual yield strengths of corroded and uncorroded bars. The yield strengths were predicted by the use of the Bethlehem Steel formula as follows:

$$[\text{UTS}] = 37,430 + 950C + 85\text{Mn} + 50P \text{ [Equation 19]}$$

Where: $[\text{UTS}]$ = ultimate tensile strength, psi

$$C = \% \text{ carbon} \times 100$$

$$\text{Mn} = \% \text{ manganese} \times 100$$

$$P = \% \text{ phosphorus} \times 100$$

The yield strengths calculated by the above formula were further confirmed by the method of Walters¹² which provides semi-linear factors for individual elements as a function of their concentration. The difference in the calculated values between the Bethlehem formula of tensile strength and the method of Walters was only 1 ksi (6.89 MPa), a 1.3% insignificant difference.

TABLE 12

Pit Depths vs Weight Loss for
#4 Reinforcing Bars Subject to Corrosion*

<u>Bar Number</u>	<u>Maximum Pit Depth, Inches</u>	<u>% Weight Loss</u>
1A	0.074	16.8%
1B	0.066	13.6%
2A	0.017	3.9%
2B	0.000	0.0%
2C	0.035	2.8%
2D	0.000	0.0%
3A	0.002	negligible
3B	0.025	5.9%
4A	0.069	12.1%
4B	0.033	6.4%
4C	0.125	11.3%
5A	0.002	negligible
5B	0.033	1.5%
5C	0.043	0.8%
5D	0.002	negligible

The predicted yield strengths and % elongation values were originally derived from the statistical analyses of Daeves¹³. The mechanical property bands for hot worked steels shown in Figure 28 are the collective representation of thousands of data points for both acid and basic carbon steels which was summary work of Sisco and other metallurgists¹⁴. The yield strength of the bar can be determined from Figure 28 by knowledge of carbon content or the tensile strength as calculated from its composition. Predicted values are useful in normalizing the tensile and yield strengths because they represent mean values which fluctuate as much as 3 ksi (21 MPa) in actual testing.

Reinforcing bars 1A, 2A, 1B, 2B, 2C, and 2D all come from the same heat, having a chemical composition of 0.31% carbon, 0.023% sulfur, 0.006% phosphorus, 0.66% manganese with the remainder iron. Reinforcing bars 3A, 3B, 4A, 4B, 4C, 5A, 5B, 5C, and 5D come from a second heat with a composition of 0.28% carbon, .026% sulfur, .007% phosphorus, 0.58% manganese with the remainder iron. The predicted mechanical properties for these two heats are listed in Table 13.

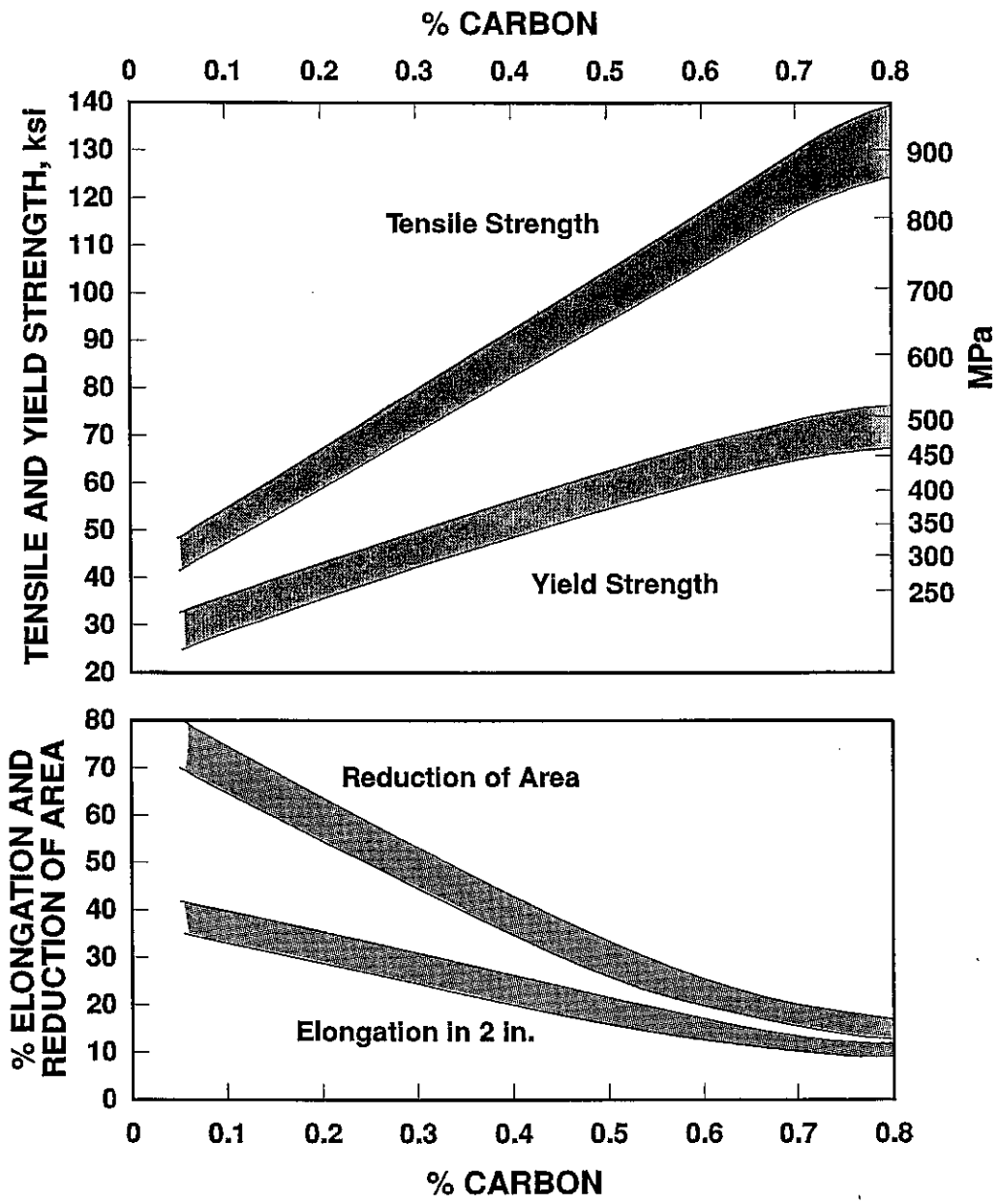


Figure 28. Effect of carbon content on the mechanical properties of hot-worked plain carbon steels (based on the data of Daeves¹³ and Sisco¹⁴).

TABLE 13

Predicted Mechanical Properties for
Two Reinforcing Bar Heats from Composition

	<u>Heat #1 (0.31% C)</u>	<u>Heat #2 (0.28% C)</u>
Tensile strength ¹	73,120 psi	69,700 psi
Yield strength ²	45,000 psi	42,000 psi
Reduction of area ²	50%	54%
Elongation ²	26%	28%

¹Predicted by the Bethlehem Steel equation.

²Determined by statistical method of Sisco, Daeves, and others^{12, 13, 14}.

These predicted values are very close to tensile test results for bars 2B, 2D, 3A and 5A showing slight corrosion or no apparent corrosion, as shown in Table 14. The predicted % elongations for the reinforcing bars are slightly higher than actual results because they are for 2" (5 cm) gage length and for smooth round bars.

Weight Losses and Mechanical Property Losses

The effect of corrosion-induced weight losses on yield strength and % elongation are plotted in Figures 29 and 30. Small changes in weight loss due to corrosion, as seen in Figures 31, 32, and 33 induced pitting and major stress concentrations, which markedly reduced ductility of the reinforcing bars. Using the normalized yield strengths based on composition, a stress concentration factor was derived by comparing % weight loss of the bar with the ratio of new bar yield strength over the actual yield strength of the corroded bar derived from testing, as shown in Figure 32. Normalized yield strengths were used because of physical difficulty in determining the original extent of corrosion and the high sensitivity of weight loss to degradation of mechanical properties.

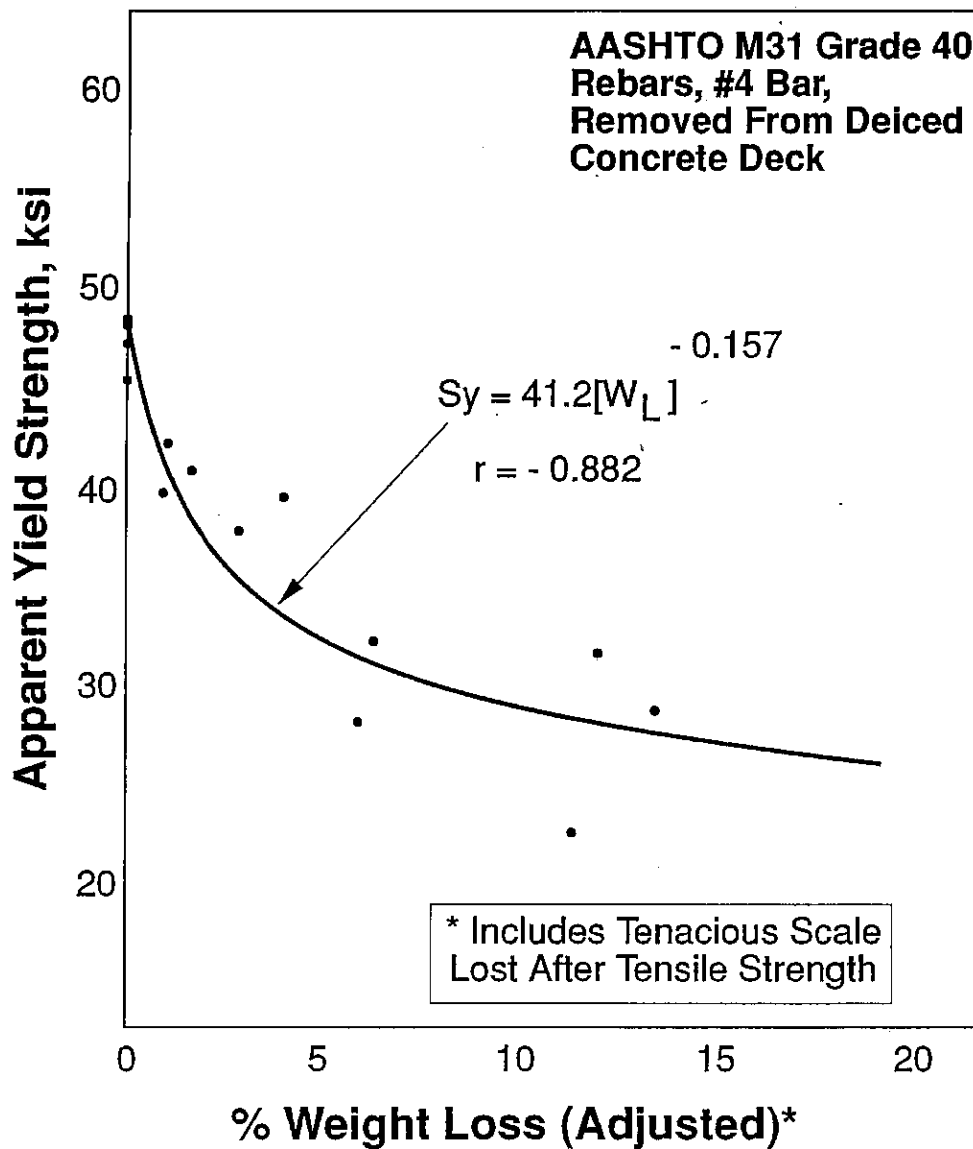


Figure 29. The loss in yield strength of a reinforcing bar as a function of percent weight loss. Note that only minor weight losses of 5% result in a 40% loss in yield strength.

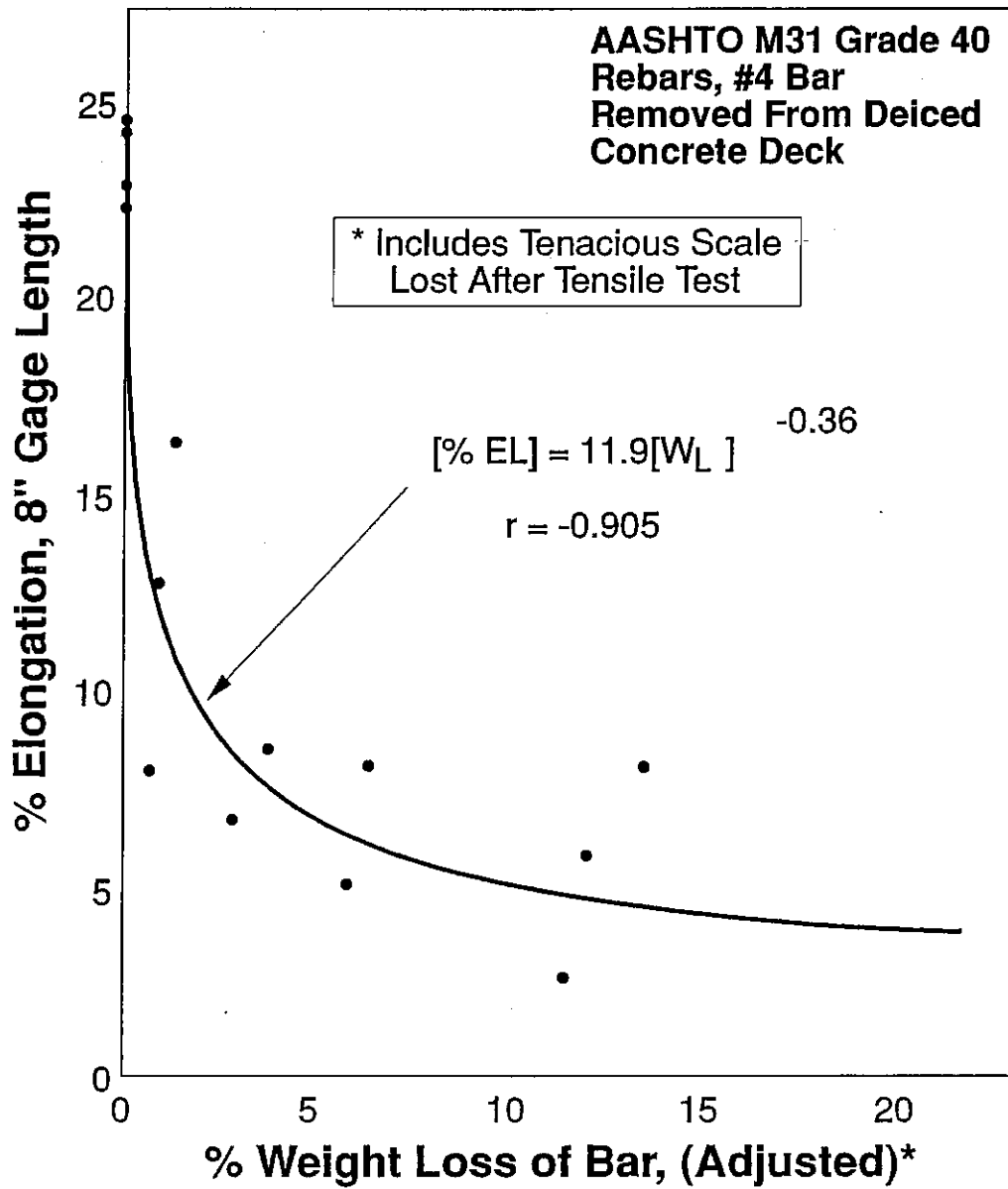


Figure 30. Loss in ductility of a reinforcing bar as a function of weight loss due to corrosion. Note that a 5% weight loss results in a 70% loss in ductility.

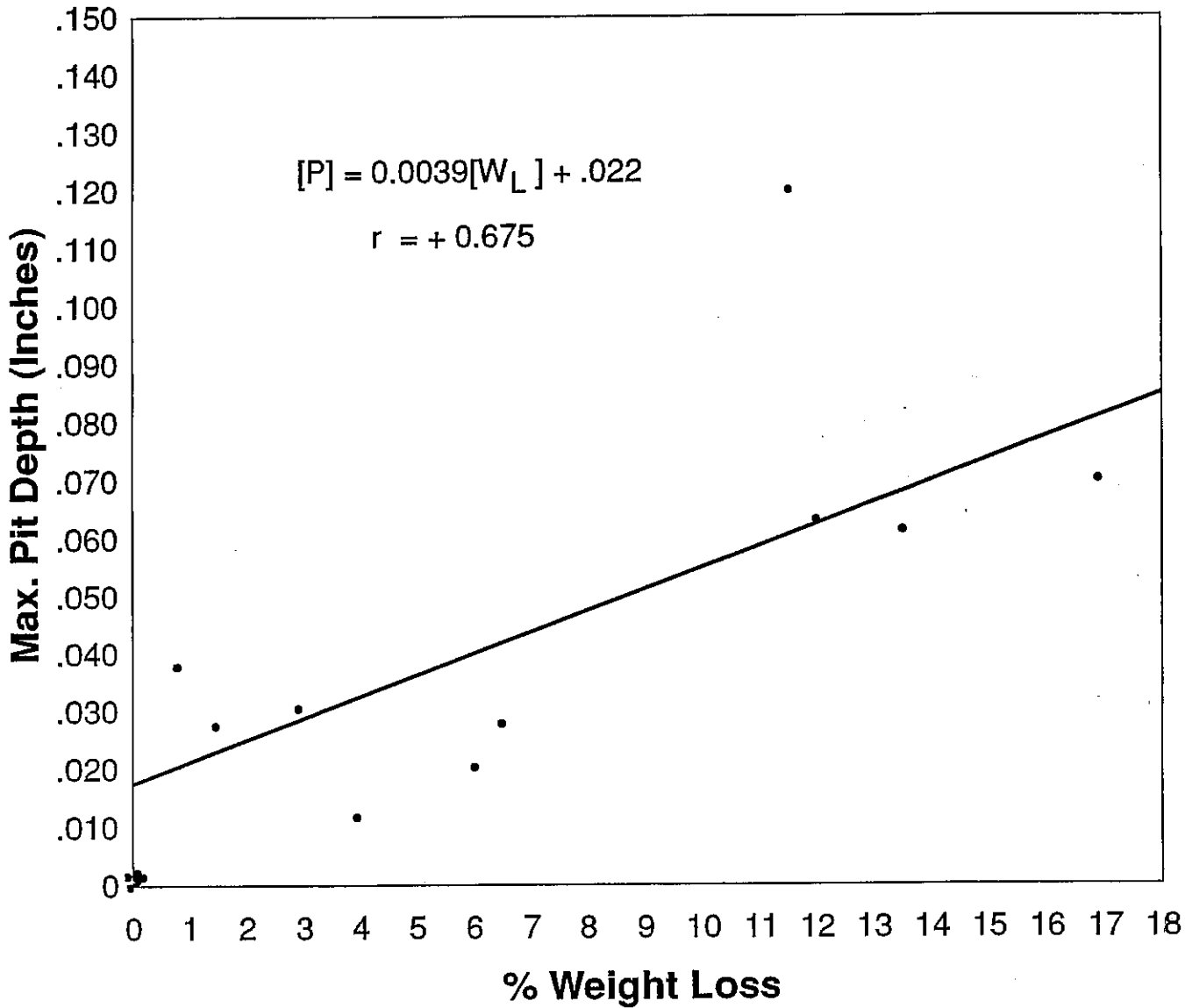


Figure 31. The maximum pit depth in a reinforcing bar as a function of its weight loss. Pit depths are subject to wide scatter. A linear function is chosen for convenience only.

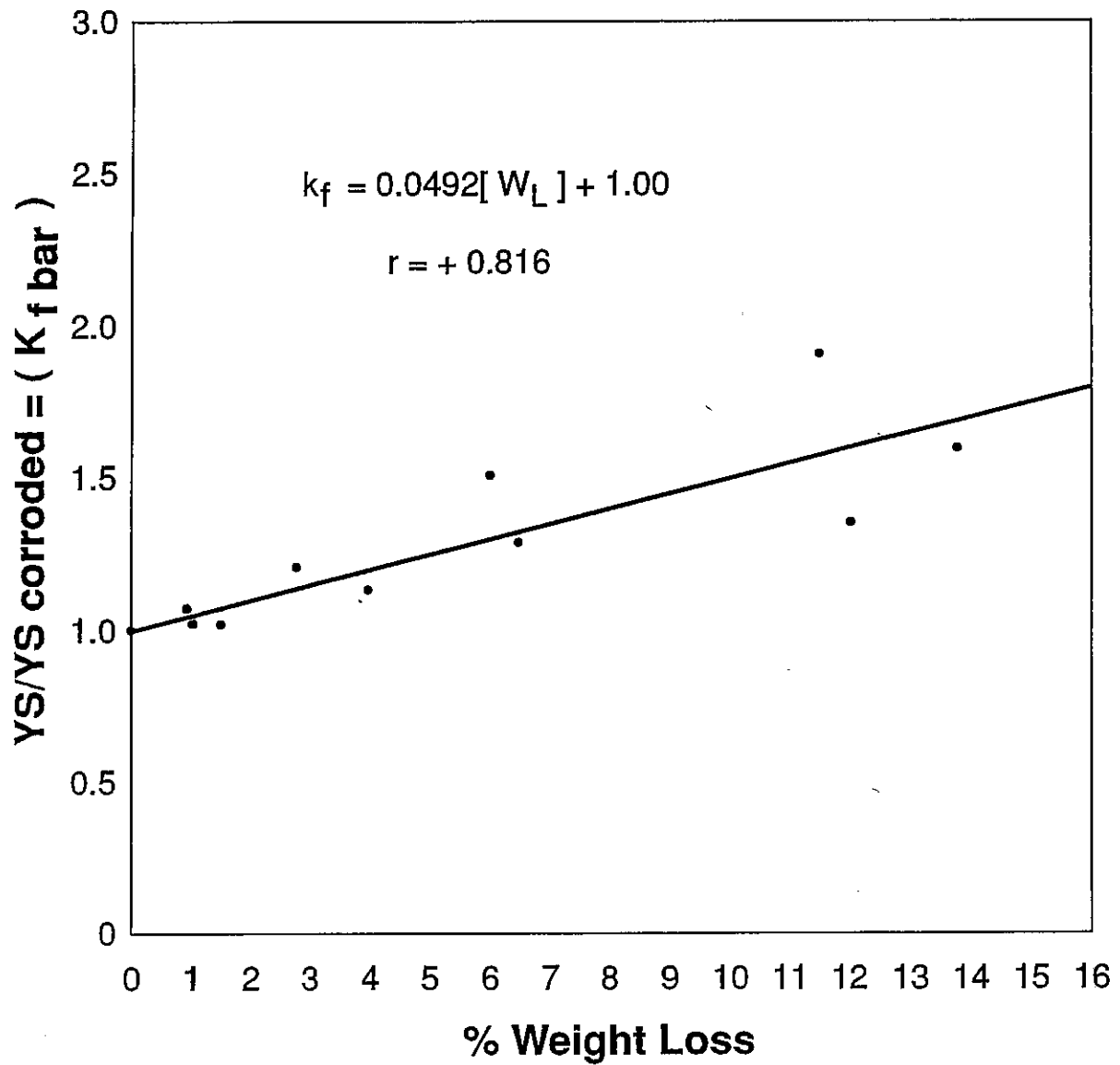


Figure 32. Stress concentration in a reinforcing bar subjected to corrosion, as represented by the ratio of its nominal yield strength to apparent yield strength when pulled in a tensile test.

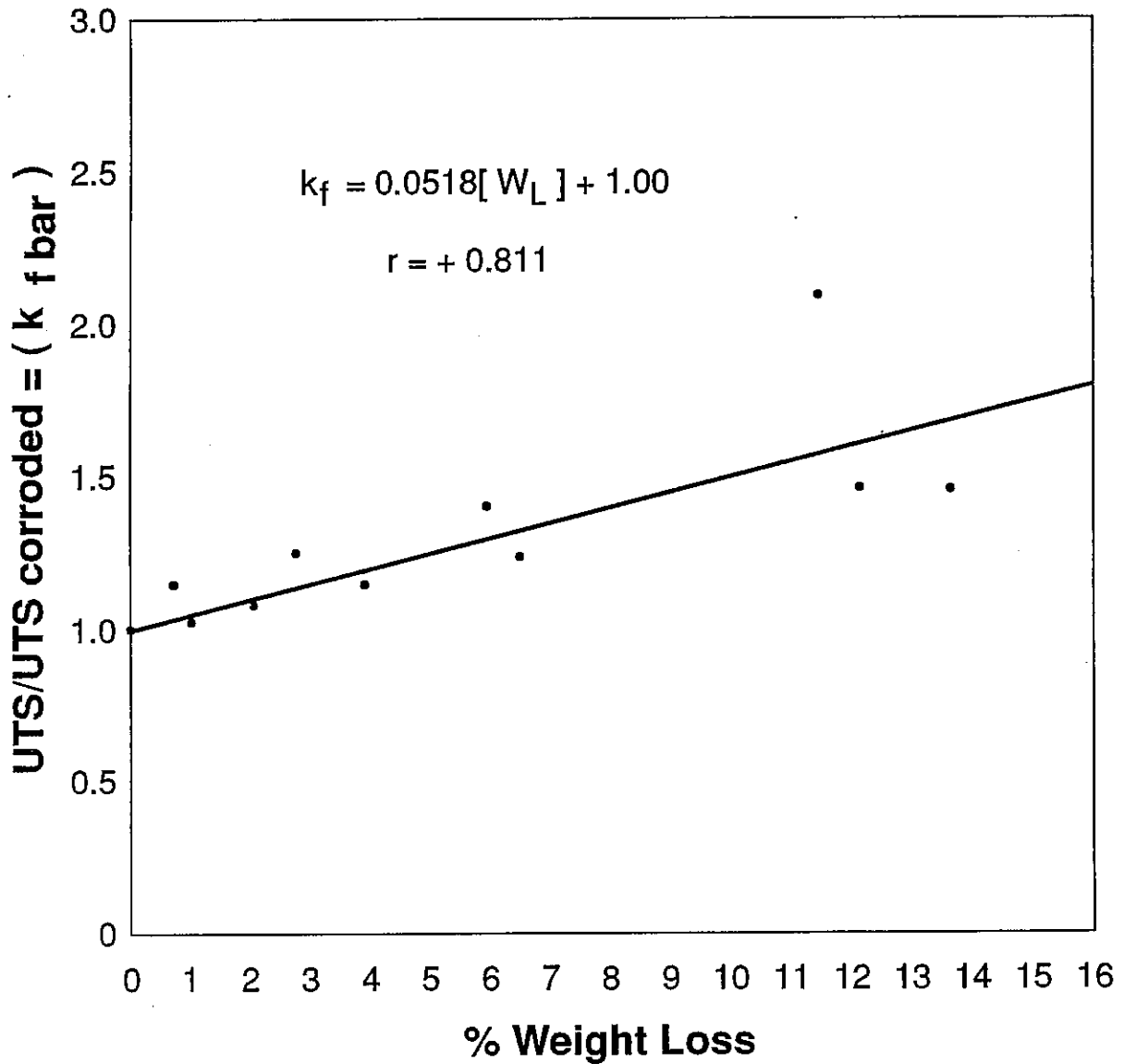


Figure 33. The stress concentration in a reinforcing bar subjected to corrosion. Similar to Figure 32, the ratio of nominal tensile strength to apparent tensile strength when pulled in a tensile test is a direct function of the bars weight loss. A 10% weight loss in the bar represents a 1.5 magnification of its nominal stress.

TABLE 14

Effects of Weight Loss on Mechanical Properties
of Reinforcing Bars

<u>Specimen Number</u>	<u>Amount of Corrosion</u>	<u>% Weight Loss</u>	<u>Yield Strength, psi</u>	<u>Tensile Strength, psi</u>	<u>% Elongation</u>
1A	extensive	16.8	--	28,900	2.0
1B	extensive	13.6	28,200	49,550	8.0
2A	considerable	3.9	39,420	62,650	8.5
2B	none	0.0	48,360	75,200	23.0
1C	light	2.8	37,800	59,750	6.7
2D	none	0.0	48,000	75,450	24.4
3A	superficial	<0.1	45,240	69,150	24.5
3B	light	5.9	27,780	49,800	5.0
4A	extensive	12.1	31,680	47,300	5.7
4B	extensive	6.4	31,920	56,350	8.0
4C	extensive	11.3	22,020	32,950	2.6
5A	slight	<0.1	47,100	72,550	22.5
5B	slight	1.5	40,800	62,950	16.5
5C	slight	0.8	39,660	61,600	7.9
5D	slight	1.0	42,120	66,950	12.8

SI Conversion 1 psi = 6.89 kPa.

Note: Predicted mechanical properties for bars 1A, 1B; 2A, 2B, 2C, 2D based on chemical composition of this heat is 45,000 psi (310 MPa) yield strength, 73,120 psi (504 MPa) tensile strength, 26% elongation; predicted properties of bars 3A, 3B; 4A, 4B, 4C; 5A, 5B, 5C, 5D based on composition of this heat was 42,000 psi (289 MPa) yield strength, 69,700 psi (480 MPa) tensile strength, 28% elongation.

COMBINED EFFECTS OF CORROSION AND FATIGUE DAMAGE
(CORROSION FATIGUE)

Definition of $[S_{corr}]$

The combined effects of corrosion and fatigue can be quantified into a single unified equation. Corrosion causes a surface degradation, and it also reduces the general sectional properties of structural members. By roughening the surface, fatigue processes are more easily initiated because of the introduction of notches and discontinuities. Similarly, by reducing sectional properties, ambient stresses rise, even though load levels are kept constant. The unified corrosion fatigue expression is:

$$N = (C/k_f)[S_{corr}]^m \quad \text{[Equation 19]}$$

Where: C = AWS/AASHTO fatigue strength coefficient

k_f = fatigue strength reduction factor

S_{corr} = stress range, adjusted for section loss

m = fatigue strength coefficient,
typically -3.26 ± 0 for structural
steels

N = number of available cycles at this
stress range

The number of cycles, n , at $[S_{corr}]$ determines overall linear damage,

Structural Shapes in Bending

For structural shapes, the term $[S_{\text{corr}}]$ is a stress range which is adjusted for section losses caused by corrosion. For a wide flange beam or an I-beam (S-shape) in bending, $[S_{\text{corr}}]$ is defined as follows:

$$[S_{\text{corr}}] = S[I_0/I_c] \quad \text{[Equation 20]}$$

Where: I_0 = initial moment of inertia

I_c = moment of inertia after corrosion is sustained

S = nominal stress range (not adjusted for corrosion losses)

A_0 = original cross-sectional area

A_c = cross sectional area, corroded state

I_c as a function of corrosion rate was previously defined by Equation [17].

For structural shapes, the term K_f is a function of pit depth or (original section thickness) / (pit radius). Pit depth is closely related to corrosion rate, where pit depth is generally about 2 x [corrosion rate] for most steels in atmospheric, intermittent, and full immersion exposures. The fatigue reduction coefficient K_f is defined for shapes and plates by pit depth:

$$K_f = 1.2 + 5.77 [p] = 1.2 + 11.54 [Rt] \quad \text{[Equations 18;19]}$$

Where: $[p]$ = pit depth
 R = corrosion rate, in/yr
 t = time, years

The fatigue reduction coefficient can also be defined more accurately by section thickness and pit radius, but this variable is more difficult to determine because extensive measurements on an area basis must be performed compared to simple measurements of pit depths.

The fatigue reduction coefficient as a function of section thickness and pit radius is defined as follows:

$$K_f = 7.54 [D/r] + 1.53 \quad \text{[Equation 12]}$$

Where: D = plate girder or structural shape thickness
r = radius of curvature of the pit

Plates or Shapes in Tension

For structural sections like angles or plates in tension, the term [S_{corr}] is defined as follows:

$$[S_{corr}] = S[A_0/A_c] \quad \text{[Equation 21]}$$

Where: A₀ = area in uncorroded state

A_c = area of section remaining after corrosion is sustained after 10 years or more

S = nominal stress range (not adjusted for corrosion)

Since corrosion rates are linear functions, section size in various structural shapes can be estimated after certain periodic intervals, such as 10, 20, 30, 40, and 50 years. The fatigue reduction factors for plates and shapes in tension are the same as those for bending as previously defined above.

Reinforcing Bars

The corrosive attack on reinforcing bars in decks with deicing salts is not entirely uniform, but tends to concentrate in the natural crevices of the bar deformations and mill scale. The loss of load carrying capacity is not a simple weight loss uniformly distributed around the bar, but a stress concentration which is a magnified loss of tensile capacity. For reinforcing bars, $[S_{corr}]$ is represented by:

$$[S_{corr}] = S[UTS/UTS_c] = S (K_{tbar}) \quad \text{[Equation 22]}$$

Where: S = nominal stress, not adjusted for corrosion

$$[UTS/UTS_c] = 0.0518[W_L] + 1.00$$

$[UTS]$ = tensile strength of bar, uncorroded

$[UTS_c]$ = tensile strength of bar, corroded

$[W_L]$ = % weight loss of bar

The fatigue reduction of the bars can be determined by pit depth or weight loss as follows:

$$K_f = 0.0492 [W_L] + 1.00 \quad \text{[Equation 23]}$$

$$[p] = 0.0039 [W_L] + .022 \quad \text{[Equation 24]}$$

Where: $[W_L]$ = % weight loss

$[p]$ = pit depth, inches

The use of weight loss is preferred over pit depth measurements since pit depths markedly vary in a corroded bar. When compared

to pit depth measurements, the extraction of corroded bars from several locations in a bridge deck and then weighing them is quite straightforward.

Cumulative Fatigue Damage

Structural members which are not corroded have a defined limit for fatigue damage as a function of stress range. However, as plates and structural shapes corrode, their surface gradually degrades from fatigue category A or B down to category D. Such degradation is a function of the environment corroding the unpainted steel, with rural environments the least aggressive and deiced river crossings the most aggressive. In Table 15a the effects of a rural exposure on an unpainted ASTM A588 plate girder starting at category B for 10, 20, 30, 40, and 50 years is shown at a corrosion rate of 0.00020 in/yr (5.08 m/yr). Again in Table 15a, the same material is contrasted with exposure to a deiced river crossing at a corrosion rate of 0.0055 in/yr (140 m/yr). For a badly degraded structure, the following equation should be used as a lower bound:

$$N = 1.76 \times 10^9 [S]^{-3.26}$$

For an upper bound, because all plate is subject to corrosion and welded structures generally have category B for fatigue, the appropriate equations are:

$$N = 1.68 \times 10^{10} [S]^{-3.26} \text{ (non-redundant)}$$

$$N = 2.47 \times 10^{10} [S]^{-3.26} \text{ (redundant)}$$

Determination of Fatigue Damage of Corroded Members

Structural members, such as plates, girders, angles, or bars are subjected to continuing damage from corrosion and traffic. Because their sections change due to corrosion, their ambient stresses increase to a value called $[S_{\text{corr}}]$. The cumulative number of stress events is summated as:

$$\sum n_i = n_1 + n_2 + n_3 + \dots$$

These events are summed up in a stress-frequency histogram gathered from strain gages by data acquisition equipment. Each stress event is then compared with the available fatigue life at that stress range by the equation $N = c/K_f [S]^{-3.26}$. The only difference between an air fatigue calculation and this procedure is that $K_f = f(R,t)$ where R is corrosion rate, and t is time. For air fatigue, $K_f = 1.0$.

Table 15b is a supplemental summary of fatigue strength coefficients for various fatigue categories based on a constant slope of $m = -3.26$. The fatigue strength coefficients were determined by taking the permissible stress ranges for various fatigue categories and back calculating with $m = -3.26$ and $N = 2 \times 10^6$. This table provides a comparison to the air fatigue coefficients which have slightly different exponents. The values for stress range at 2×10^6 for the various fatigue categories are taken from AASHTO Standard Specifications for Highway Bridges, 15th Edition, 1992, Table 10.3.1A.

TABLE 15a

Effects of Environment on Fatigue Coefficients
of Unpainted ASTM A588 Plate Girders

Rural Environment
(Corrosion rate = 0.0002 in/yr)

Time, yrs	k_f	Fatigue Coefficients		Equivalent AWS Fatigue Category	
		Non-Redundant	Redundant	Non-Redundant	Redundant
0	1.00	1.68×10^{10}	2.47×10^{10}	Category B	B
10	1.22	1.38×10^{10}	2.02×10^{10}	Category B	B
20	1.25	1.34×10^{10}	1.98×10^{10}	Category B	B
30	1.27	1.32×10^{10}	1.94×10^{10}	Category B	B
40	1.29	1.30×10^{10}	1.91×10^{10}	Category B	B
50	1.32	1.27×10^{10}	1.87×10^{10}	Category B	B

Deiced River Crossing
(Corrosion rate = 0.0055 in/yr)

		Non-Redundant	Redundant	Non-Redundant	Redundant
0	1.00	1.68×10^{10}	2.47×10^{10}	Category B	B
10	1.83	9.18×10^9	1.39×10^{10}	Category B/C	B
20	2.47	6.80×10^9	1.00×10^{10}	Category B/C	B/C
30	3.10	5.42×10^9	7.97×10^9	Category B/C	C
40	3.74	4.49×10^9	6.60×10^9	Category C	C
50	4.37	3.84×10^9	5.65×10^9	Category C	C/D

Note: $k_f = 1.2 + 11.54[Rt]$ where R = corrosion rate in inches/yr and t = time, years.

TABLE 15b

Revised Fatigue Strength Coefficients for
Various Fatigue Categories with a Constant Slope
($m = -3.26$)

Redundant Structures

<u>Equivalent Fatigue Category</u>	<u>Fatigue Strength Coefficient, C</u>
A	6.32×10^{10}
B	2.47×10^{10}
C	8.56×10^9
D	3.64×10^9

Non-Redundant Structures

A	6.32×10^{10}
B	1.68×10^{10}
C	3.64×10^9
D	1.76×10^9

As an example, a 20-year old multi-girder weathering steel bridge spans a river crossing in the Chicago metro area. The bridge is frequently deiced. The girders are welded ASTM A588. The bridge is exhibiting substantial corrosion, particularly on the lower flanges of the girders, and a decision must be made whether the bridge should be painted or not. If left unpainted, what would be the significant damage sustained over the next 10 years compared to painting the bridge?

For purposes of simplicity, it is assumed that there is no traffic growth, and that the original stress ranges are those found in Table 4, and the number of cycles at these stress ranges are approximately the same. The available fatigue life at the starting point is $N = 2.47 \times 10^{10} [S]^{-3.26}$, which is the fatigue equation for Category B. However, after 20 years of exposure to deicing salts over a river crossing, the weathering steel sustains a corrosion rate of 0.0055 in/yr. This results in a $k_f = 1.2 + 11.59 [Rt] = 2.47$. After 20 years, the available fatigue life is reduced to:

$$N = 2.47 \times 10^{10} / (2.47) [S]^{-3.26} = 1 \times 10^{10} [S]^{-3.26}.$$

If the structure is not painted for another 10 years, then:

$$K_f = 1.2 + 11.59 [.0055(30)] = 3.11, \text{ resulting in a downwardly revised corrosion fatigue expression of}$$

$$N = 7.94 \times 10^9 [S]^{-3.26}.$$

Not only did available fatigue life change due to surface changes, but the stress ranges also increased because of section loss due to corrosion. The moment of inertia of the plate girder also decreased. Assuming the plate girder is approximately

equivalent to a 36 x 12 x 160 lbs/ft WF, its original moment of inertia was 9,738 in⁴. By use of equation [17] and a corrosion rate of 0.0055 in/yr, the moment of inertia decreases to 7,208 in⁴. Over this twenty-year period, the stress ranges have increased by 26%. In another 10 years, if still unpainted, stresses will be 38% greater. In the calculation of Table 10, the amount of damage incurred in 10 years to a bridge painted after 20 years of exposure is compared to being left unpainted for 30 years. In the first damage column, (painted after 20 years) the bridge sustains damage equivalent to 9.3% of its life in 20 years. However, by not painting the bridge for another 10 years, the bridge sustains an additional 12.8% damage to its life. By not painting for 10 more years, a total of 22.1% damage occurs. If the bridge is painted after 20 years of exposure, 19.4% total damage is sustained. If painting was deferred beyond 10 years or more, greater amounts of damage would be sustained.

In the 10 years of comparison, since the 22.1% damage sustained by an unpainted bridge is only slightly greater than 19.4% damage for a painted bridge, the cost of painting may not justify such a marginal improvement in fatigue life. Each calculation, depending on traffic growth and amount of permit loads the bridge sustains, will determine the extent of cumulative damage and whether painting is justified on a cost-benefit basis.

These procedures for the determination of corrosion-induced degradation of fatigue life have particular significance in the light of recent dramatic changes in the cost of painting structural steel. In the 1970s, it typically cost \$0.12/ft² (\$1.29/m²) to paint structural steel. By the late 1980s, costs

had escalated at a rate of 12%, largely due to inflation of construction costs, to 1.62/ft² (17.42/m²). The costs of painting existing bridges now include lead containment, worker protection, blood lead level monitoring, and the disposal of wastes containing lead. Over the past 5 years, unit costs have risen to approximately \$6.00/ft² (\$64.50/m²).¹⁵

The Connecticut DOT¹⁵ compared the cost of painting existing corroded structures coated with red lead and, in several instances, found that complete replacement of the structural steel was more economical. The implication of this finding is that a corroding structure coated with red lead should be first evaluated for pit depth, section loss and resultant fatigue category, and then determine its fatigue life by factoring in its traffic spectrum. Many structures may have significant fatigue life remaining, and painting them may be largely a cosmetic action in certain instances. At a certain point when fatigue life of the bridge is seriously shortened due to increasing traffic, complete steel replacement may actually be more economical than painting the existing corroded steel.

TABLE 16
 Damage Comparison of Whether an Unpainted Weathering Steel
 Bridge Exposed for 20 Years Should be Painted

Original Stress Range, ksi	No. of Stress Cycles Per Year	No. of Stress Cycles In 20 Yrs.	Available Cycles Unpainted = $1 \times 10^{10} [S]^{-3.26}$	Damage After 20 Yrs., n_i/N_i
1.0	1,000,000	20 x 10 ⁶	1 x 10 ¹⁰	.002
2.0	350,000	7 x 10 ⁶	1.04 x 10 ⁹	.007
3.0	150,000	3 x 10 ⁶	2.78 x 10 ⁸	.011
4.0	40,000	8 x 10 ⁵	1.09 x 10 ⁸	.007
5.0	30,000	6 x 10 ⁵	5.26 x 10 ⁷	.011
6.0	25,000	5 x 10 ⁵	2.91 x 10 ⁷	.017
7.0	20,000	4 x 10 ⁵	1.75 x 10 ⁷	.023
8.0	5,000	10 x 10 ⁴	1.14 x 10 ⁷	.009
9.0	2,500	5 x 10 ⁴	7.75 x 10 ⁶	.006
				<u>.093</u>

New Stress Range After 20 Yrs.	Available Cycles After 30 Yrs., $N = 7.94 \times 10^9 [S]^{-3.26}$	No Stress Cycles In 10 Yrs.	Available Cycles if Painted at 20 Yrs., $N = 1 \times 10^{10} [S]^{-3.26}$
1.3	3.38 x 10 ⁹	10 x 10 ⁶	4.30 x 10 ⁹
2.7	3.12 x 10 ⁸	3.5 x 10 ⁶	3.92 x 10 ⁸
3.8	1.02 x 10 ⁸	1.5 x 10 ⁶	1.29 x 10 ⁸
5.0	4.18 x 10 ⁷	4 x 10 ⁵	5.26 x 10 ⁷
6.3	1.97 x 10 ⁷	3 x 10 ⁵	2.48 x 10 ⁷
7.6	1.07 x 10 ⁷	2.5 x 10 ⁵	1.34 x 10 ⁷
8.8	6.62 x 10 ⁶	2 x 10 ⁵	8.34 x 10 ⁶
10.1	4.22 x 10 ⁶	5 x 10 ⁴	5.32 x 10 ⁶
11.3	2.93 x 10 ⁶	2.5 x 10 ⁴	3.69 x 10 ⁶

10-Year Damage if Painted After 20 Yrs.	10-Year Damage If Not Painted After 20 Yrs.
.002	.003
.009	.011
.012	.015
.008	.010
.012	.015
.018	.023
.024	.030
.009	.012
.007	.009
<u>.101</u>	<u>.128</u>

Note: Calculation assumes (a) no increase in traffic as a function of time (0% growth); (b) bridge is non-redundant construction, is a deiced river crossing with ASTM A588 weathering steel girders.

SUMMARY AND CONCLUSIONS

1. Bridges are subject to the simultaneous action of fatigue and corrosion. The extent of corrosion is dependent on the bridge's location and the proximity of its main load carrying members to large bodies of water, major rivers, or the condensation of moisture containing atmospheric pollutants or dust emissions. In rural and suburban locations, the application of deicing salts is a major contributing factor to corrosion of bridge decking and structural members.
2. Pitting and crevice corrosion have the most profound effects on the fatigue life of bridges, affecting wide flange girders, diaphragms, floor beams, truss chords, reinforcing bars, and other main load-carrying members.
3. Fatigue damage in dry air can be predicted by analytical methods or measured directly by the placement of strain gages on critical or main load-carrying members. The resulting data collection of live loads is put into a stress-frequency histogram to provide a daily count of traffic. Fatigue damage over a period of years is then assessed by either integrating the area under the curve or by individually comparing each stress increment with the available number of cycles for that stress range using the relationship $N = C[S]^m$ for the detail in question if no corrosion is involved. The amount of

cumulative damage is determined by the linear damage rule. The amount of fatigue each detail can sustain depends on its geometry, notch severity, and residual stress. These detail effects on fatigue are represented by fatigue categories, descending in order from A to E.

4. Corrosion largely affects the fatigue of critical main load-carrying members by surface degradation through pitting and section loss in wet-dry cycles. Corrosion is further accelerated by complete immersion. Pitting rates in most common structural steels are approximately twice the corrosion rate for most environments. A generalized corrosion fatigue damage equation is proposed to account for reduced crack initiation time and the changes in ambient stresses caused by corrosion due to section loss in beams, gusset plates, channels, and angles. The use of a fatigue reduction factor k_f , based on average corrosion rate, is also proposed. The corrosion fatigue relationship which defines the amount of available stress cycles at various stress ranges is $N = (C/k_f) [S]^{-3.26}$ where C is the initial AWS fatigue category coefficient for fatigue category A or B and k_f is the fatigue reduction factor, which is a function of the product of corrosion rate and time of exposure, $k_f = 1.2 + 11.59 [Rt]$. The individual stress ranges are determined by corrosion-induced changes in section or by stress concentration effects in the section where $[S] = f [S_{corr}]$.

5. Reinforcing bars, even if subject to minor weight losses due to corrosion, tend to concentrate attack in localized areas, resulting in major losses of ductility and yield strength. For example, a 10% weight loss in an AASHTO M31 Grade 40 #4 rebar caused a drop in typical yield strength from 45 ksi to 29 ksi and ductility losses from 23% elongation to 5% elongation. Such severe losses indicate marked degradation of load bearing capacity and very limited plasticity once the bars have yielded under load.

6. For bridges in rural and suburban locations, and for highway and rail crossing features not involving water, corrosion fatigue is not a major problem. However, for bridges crossing large bodies of water, rivers, and streams where condensation, immersion, high humidity, dust and debris, pollution or deicing salts are involved, corrosion fatigue can range from significant to severe.

7. The unified corrosion fatigue equation for structural steel, $N = C/k_f[S]^m$ developed in this report is very useful in (a) predicting corrosion fatigue damage, (b) the effects of delayed painting and maintenance on fatigue, and (c) evaluation of the general load-carrying capacity for steel bridges. These findings are particularly pertinent when considering the current high cost of painting structures coated with red lead. The values for C, k_f and m were determined in this study. Other equations developed in this work provide direct, quantifiable indications of potential damage in reinforced concrete bridges when reinforcing bars are corroded.

REFERENCES

1. C. Hahin and J. South, Accurate and Rapid Determination of Fatigue Damage in Bridge Superstructures, Illinois Department of Transportation, Physical Research Report No. 106, Springfield, Illinois, December 1992.
2. D. McAdam, Proceedings ASTM Vol. 27, No. 2, 1927, p. 102.
3. A. V. Karpov, Metals and Alloys, Dec. 1939: p. 381.
4. Battelle Memorial Institute, Prevention of Fatigue of Metals, Wiley, New York, 1941.
5. H. H. Uhlig and R. Reve, Corrosion and Corrosion Control, Wiley, New York, 1975, pp. 155-157.
6. P. Albrecht, C. Shabshab, W. Li and W. Wright, Remaining Fatigue Strength of Corroded Steel Beams, International Association for Bridges and Structural Engineering Workshop Lausanne, Switzerland, 1990.
7. Structural Welding Code - Steel, American Welding Society, Miami, Fl., 1984.
8. J. Barsom and S. Rolfe, Fracture and Fatigue Control in Structures, 2nd Edition, Prentice-Hall, Englewood Cliffs, NJ, 1987.
9. F. Fink and W. Boyd, The Corrosion of Metals in Marine Environments, DMIC Report 245, Defense Metals Information Center, Columbus, OH, 1970, pp. 22-25.
10. R. Peterson, Stress Concentration Factors, John Wiley, New York, 1974, pp. 20-79.
11. National Bureau of Standards, Underground Corrosion, Department of Commerce, Washington, DC, 1945.
12. F. Walters, Jr., Transactions AIME, Vol. 154, 1943, p. 407.
13. K. Daeves, Mechanical Properties of Basic and Acid Steels, Stahl Und Eisen, Vol. 50, 1930, pp. 1353-1356.
14. F. Sisco, Properties of Hot Worked Steels, The Alloys of Iron and Carbon, Vol. II, McGraw-Hill, New York, 1937, pp. 81-109.
15. L. B. Castler, The Lead Paint Dilemma, Journal of Protective Coatings and Linings, July 1994, pp. 54-62.

2847i